British Geological Survey
NATURAL ENVIRONMENT RESEARCH COUNCIL

Project EURISGIC: Worst Case Scenarios (Technical Note D5.1)

Earth Hazards and Systems Programme

CR Report CR/14/004

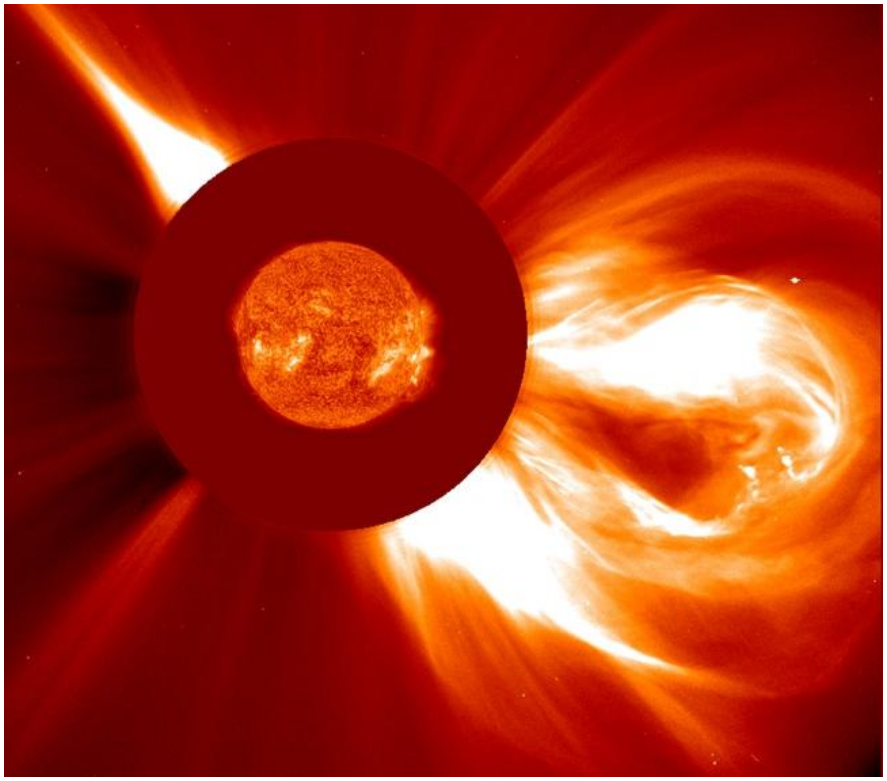

BRITISH GEOLOGICAL SURVEY

Earth Hazards and Observatories PROGRAMME

CR REPORT CR/14/004

Project EURISGIC: Worst Case Scenarios (Technical Note D5.1)

Alan W P Thomson (Editor), Ciaran Beggan, Gemma Kelly, Orsi Baillie, Ari Viljanen, Chigomezyo Ngwira

Keywords

Report; Geomagnetism; EURISGIC; Worst Case Scenarios.

Front cover

Composite image of Coronal Mass Ejection from the Sun (Dec 2003). Courtesy of SOHO consortium. SOHO is a project of international cooperation between ESA and NASA.

Bibliographical reference

THOMSON, A. W. P. ET AL 2014. Project EURISGIC: Worst Case Scenarios (Technical Note D5.1). *British Geological Survey Report*, CR/14/004. 40pp.

Keyworth, Nottingham British Geological Survey 2014

BRITISH GEOLOGICAL SURVEY

The full range of our publications is available from BGS shops at Nottingham, Edinburgh, London and Cardiff (Welsh publications only) see contact details below or shop online at www.geologyshop.com

The London Information Office also maintains a reference collection of BGS publications, including maps, for consultation.

We publish an annual catalogue of our maps and other publications; this catalogue is available online or from any of the BGS shops.

The British Geological Survey carries out the geological survey of Great Britain and Northern Ireland (the latter as an agency service for the government of Northern Ireland), and of the surrounding continental shelf, as well as basic research projects. It also undertakes programmes of technical aid in geology in developing countries.

The British Geological Survey is a component body of the Natural Environment Research Council.

British Geological Survey offices

BGS Central Enquiries Desk

Tel 0115 936 3143 Fax 0115 936 3276

email enquiries@bgs.ac.uk

Kingsley Dunham Centre, Keyworth, Nottingham NG12 5GG

Tel 0115 936 3241 Fax 0115 936 3488

email sales@bgs.ac.uk

Murchison House, West Mains Road, Edinburgh EH9 3LA

Tel 0131 667 1000 Fax 0131 668 2683

email scotsales@bgs.ac.uk

Natural History Museum, Cromwell Road, London SW7 5BD

Tel 020 7589 4090 Fax 020 7584 8270

Tel 020 7942 5344/45 email bgslondon@bgs.ac.uk

Columbus House, Greenmeadow Springs, Tongwynlais, Cardiff CF15 7NE

Tel 029 2052 1962 Fax 029 2052 1963

Maclean Building, Crowmarsh Gifford, Wallingford OX10 8BB

Tel 01491 838800 Fax 01491 692345

Geological Survey of Northern Ireland, Colby House, Stranmillis Court, Belfast BT9 5BF

Tel 028 9038 8462 Fax 028 9038 8461

www.bgs.ac.uk/gsni/

Parent Body

Natural Environment Research Council, Polaris House, North Star Avenue, Swindon SN2 1EU

Tel 01793 411500 Fax 01793 411501

www.nerc.ac.uk

Website www.bgs.ac.uk

Shop online at www.geologyshop.com

Foreword

This report is the published product of a study by the British Geological Survey (BGS) as part of the EURISGIC EC FP7 project (BGS projects NEE4272SF and NEE3710F) into the risk from geomagnetically induced currents (GIC) in high voltage power systems across Europe.

A review of BGS and project partners' research and publications into space weather and GIC 'worst case scenarios' is presented. This work has mostly already appeared in the peer reviewed literature, but is collected here to provide an easy overview of the EURISGIC team's collective achievements during the project lifetime.

Acknowledgements

The research leading to these results has received funding from the European Community's Seventh Framework Programme (FP7/2007-2013) under grant agreement no. 260330.

Geomagnetic and geoelectric data provided by worldwide institutes, for example through INTERMAGNET, is gratefully acknowledged.

Full IPR for the results provided by FMI (section 3) and NASA and the Catholic University of America (section 4) rest with these organisations. The editor thanks the contributors from these institutes for permission to include their results in this document.

Contents

FIGURES

TABLES

1 Introduction

The overall objective of Work Package 5 of the EURISGIC project (see website eurisgic.eu) is defined as being:

"Estimate the largest possible GIC flowing anywhere in the European high-voltage power grid, based on archive data."

This document is a technical note (deliverable item D5.1) for the results of this work package.

For each of the project team members participating in the work package (FMI – Finland; Neurospace – Sweden; IRF – Sweden; NASA and Catholic University of America - USA; BGS - UK) we summarise activities related to worst case scenario modelling: activities such as research into extreme event statistical methods, theoretical extreme event modelling and individual (historical and hypothetical) event studies.

We note that research is continuing and therefore some results reported here are subject to further confirmation in published scientific journals.

2 Worst Case Scenario Research at BGS

Recent research at BGS has focussed on applying the technique of extreme value statistics (EVS) to geomagnetic and, more recently, to geoelectric field data. EVS analysis involves the fitting of a generic function – in this case the generalised Pareto distribution (GPD) – to the tail of a distribution of data. From the best functional fit, such characteristics as the return level and return period for extreme events can be deduced, along with uncertainties.

Estimates of extreme values and their return intervals can then be used to investigate the extremes in geomagnetically induced currents (GIC) in, for example, the UK or European high voltage transmission grid, by means of a model of each grid and a model of the surface electric field generated by the extreme magnetic variations.

Some BGS results were previously reported in EURISGIC technical note D1.3 (in section 5), given in BGS report number CR/12/024 (Beggan and Thomson, 2012). These results are not repeated here.

There are 4 specific results we do report here:

- EVS as applied to European geomagnetic observatory data – in section 2.1
- EVS as applied to global geomagnetic observatory data – in section 2.2
- EVS as applied to Nagycenk geoelectric field data – in section 2.3
- Extreme GIC in the UK grid, resulting from extreme European magnetic variations – in section 2.4

2.1 EVS AND EUROPEAN GEOMAGNETIC OBSERVATORY DATA

In the paper by Thomson *et al.* (2011), EVS was applied to a number of decades of one-minute mean magnetic data from 28 magnetic observatories in Europe, to provide a preliminary exploration of the extremes in magnetic field variations and their one-minute rates of change. These extremes were expressed in terms of the variations that might be observed every 100 and 200 years in the horizontal strength (*H*) and in the declination (*D*) of the field.

Before fitting a GPD to each data set, Thomson *et al.* first determined a threshold to mark the onset of extreme behaviour. The ideal threshold should be low enough to allow for a meaningful

number of samples, but high enough that the modified 'scale' parameter of the GPD is approximately constant and the GPD 'shape' parameter approximately linear (within error-margins), above the chosen threshold. It was found that setting the threshold at the 99.97th percentile proved reasonable for each variable at most observatories.

Clusters of extreme values occur during geomagnetic storms. These can be where the storm maximum is accompanied closely in time with other near-maxima. Including these near-maxima in the data skews the extreme value statistics in the following sense: we wish to identify the return period for each major event, i.e. single magnetic storm, in the sense that one would describe 13th March 1989, or 30th October 2003 as a single event, even though there was much complex structure in the activity that occurred on each of these days. By experimenting with a de-clustering algorithm with a variable de-cluster length (from three hours to one week), Thomson *et al.* showed that the return level is generally only weakly dependent on the de-cluster length for most observatories, but that de-clustering increases the extrapolated return level, compared to not applying de-clustering.

For each observatory Thomson *et al.* computed the peak residual and peak rate-of-change predicted by the observatory GPD to be exceeded once within periods of 100 and 200 years, from examination of the return-level statistics. The results for the four time-series are summarised in Figures 2.1 (*H* residual), 2.2 (d*H*/dt), 2.3 (*D* residual) and 2.4 (d*D*/dt). Note that the *H* residual is computed from the north (*X*) and east (*Y*) component as the square root of the sum of squares in *X* and *Y*. d*H*/dt is then computed through the change in *H*, minute to minute, and not from d*X*/dt and d*Y*/dt. Thus d*H*/dt may underestimate the strength of changes in the vector horizontal field. (Future work will investigate the vector d*H*/dt.)

In Figures 2.1-2.4 Thomson *et al.* do not consider any local time, or longitude, dependence as significant as the latitude dependence. During any individual storm, *when* the peak electrojet activity occurs will define *where* the extreme is localised in longitude (if it is localised). However at the time scales of years between single storms and with de-clustering of 12 hours or more, such small time dependency of a few hours is probably not significant.

Thomson *et al.* found that both measured and extrapolated extreme values generally increase with geomagnetic latitude though there is a marked maximum in estimated extreme levels between about 53 and 62 degrees north. At typical mid-latitude European observatories (55-60 degrees geomagnetic latitude) compass variations may reach approximately 3-8 degrees/minute, and horizontal field changes may reach 1000-4000 nT/minute, in one magnetic storm once every 100 years. For storm return periods of 200 years the equivalent figures are 4-11 degrees/minute and 1000-6000 nT/minute. More details are given in Table 5-1.

From the GPD fits to each observatory data set Thomson *et al.* found that, for nearly all observatories and data types, the GPD shape parameter is positive, but generally less than one, and exceeds its standard error. This suggests that extreme geomagnetic activity is not bounded by some maximum, but follows either a Gumbel or Frechet distribution, i.e. the probability of increasingly higher values diminishes exponentially or polynomially with value. The consequence of this is that over even longer return periods, compared for example with 200 years, higher extreme values can be expected to occur.

Table 1. Estimated 100 and 200 year maxima in each of *H*, d*H*/dt, *D* and d*D*/dt between 55 and 60 geomagnetic degrees north, summarised from Figures 2-1 to 2-4. Figures in parentheses apply where Valentia (Ireland) observatory data are excluded, on the basis that these data seem anomalously low, compared to others of similar latitude.

	***H* (nT)**	**d*H*/dt (nT/min)**	***D* (degrees)**	**d*D*/dt (deg/min)**
100 Year Return	2000-5000 (4000-5000)	1000-4000 (1500-4000)	4-15 (7-15)	3-8 (5-8)
200 Year Return	3000-6500 (4500-6500)	1000-6000 (2000-6000)	5-20 (10-20)	4-11 (7-11)

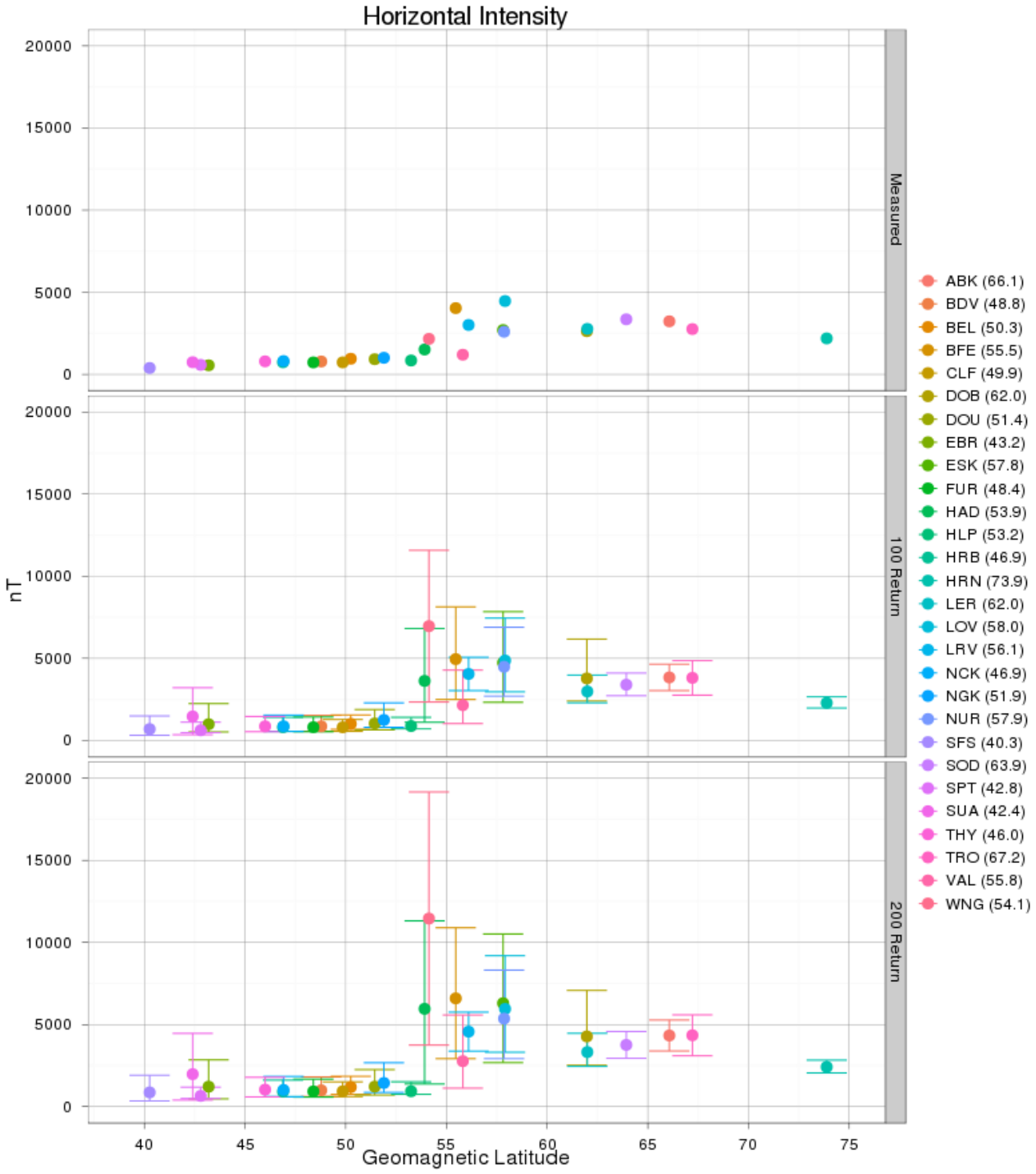

Figure 2-1: The measured maximum for each observatory (top), and estimated 100-year (middle) and 200-year (bottom) return-levels, for *H*, in nT, as a function of geomagnetic latitude. 95% confidence limits are shown.

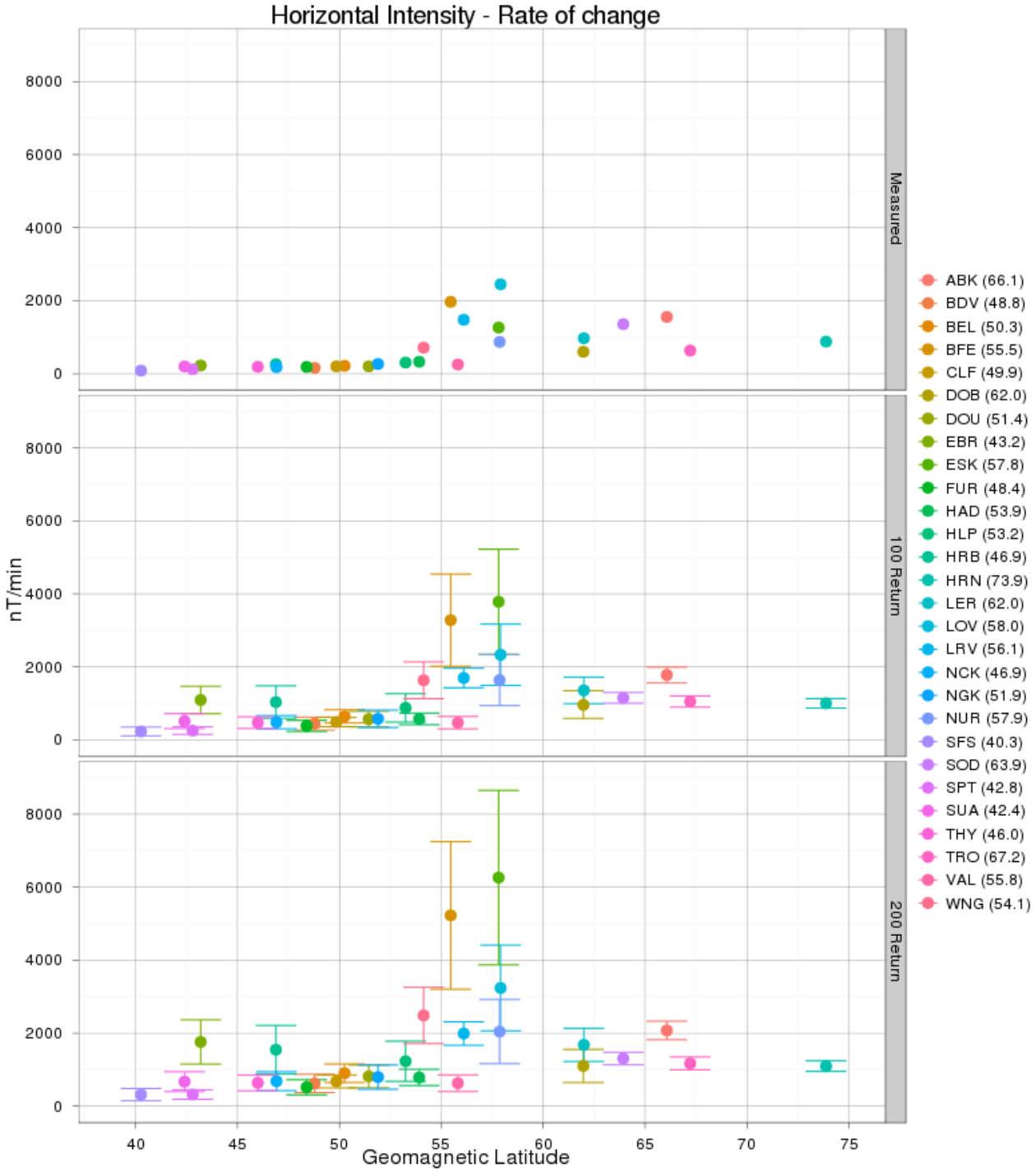

Figure 2-2: The measured maximum for each observatory (top), and estimated 100-year (middle) and 200-year (bottom) return-levels, for d*H*/dt, in nT/min, as a function of geomagnetic latitude. 95% confidence limits are shown.

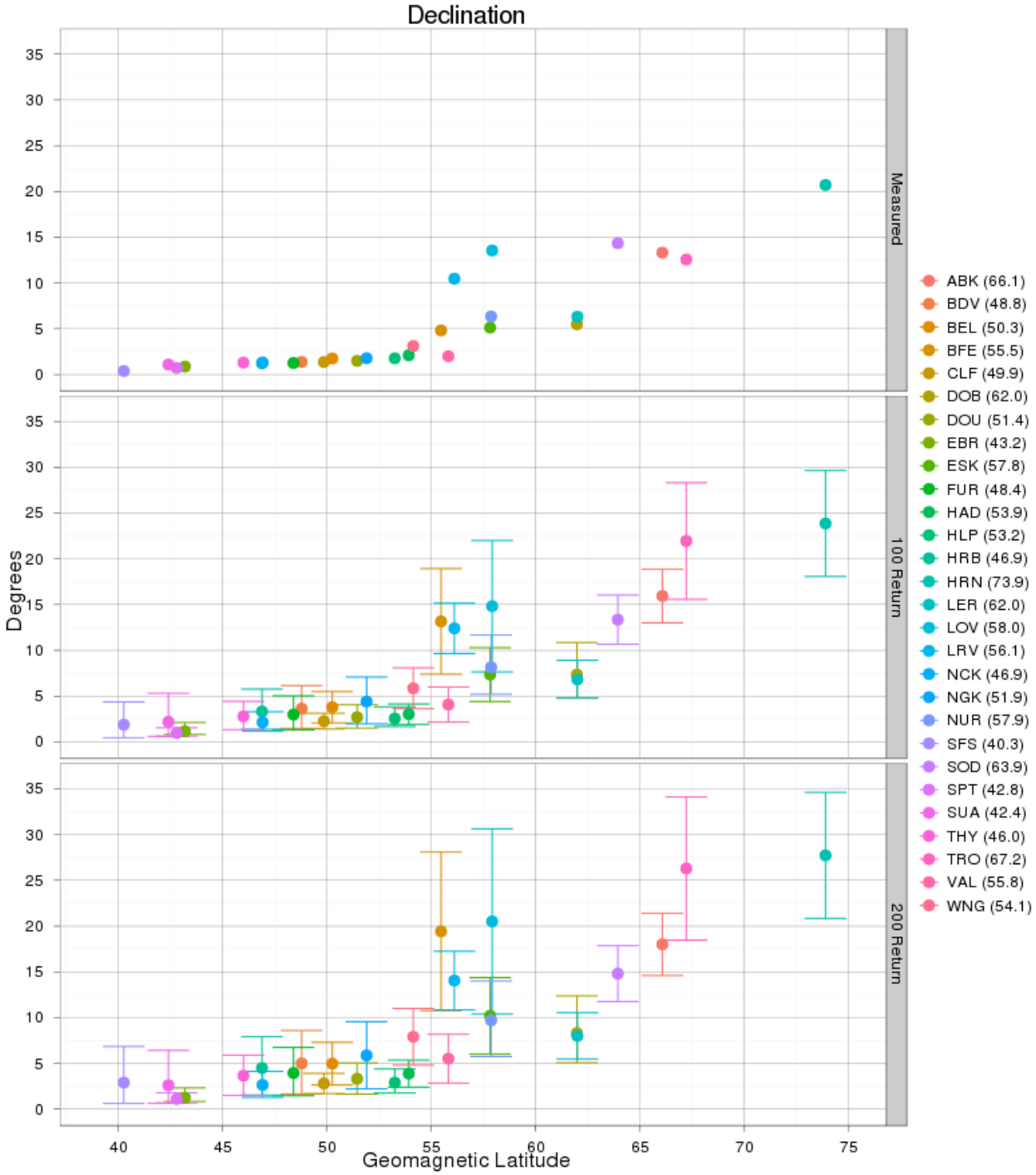

Figure 2-3: The measured maximum for each observatory (top), and estimated 100-year (middle) and 200-year (bottom) return-levels, for *D*, in degrees, as a function of geomagnetic latitude. 95% confidence limits are shown.

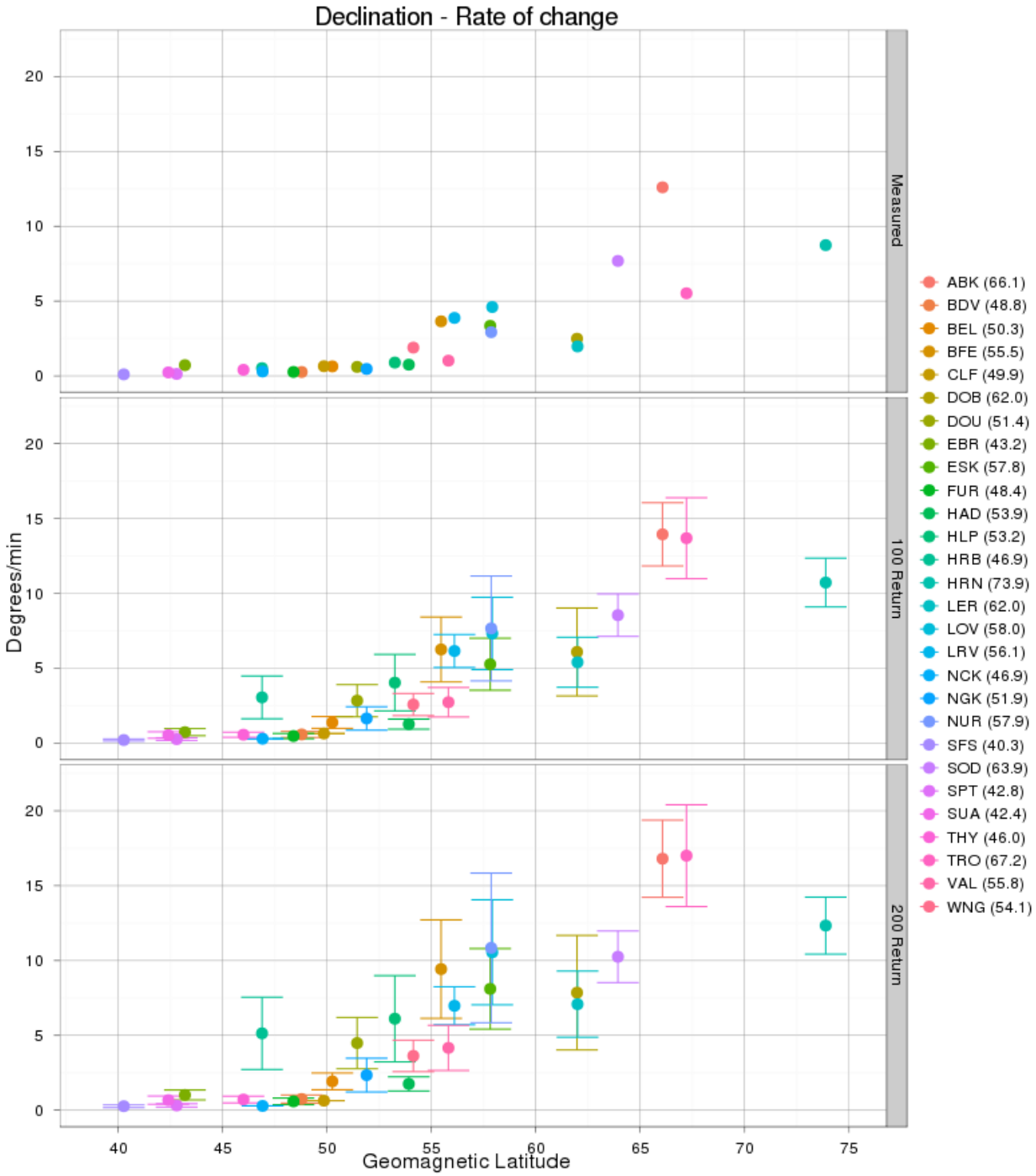

Figure 2-4: The measured maximum for each observatory (top), and estimated 100-year (middle) and 200-year (bottom) return-levels, for d*D*/dt, in degrees/min, as a function of geomagnetic latitude. 95% confidence limits are shown.

2.2 EVS AND GLOBAL GEOMAGNETIC OBSERVATORY DATA

Although the results from the European wide EVS analysis (Thomson *et al*., 2011, and as summarised in the previous section) show some consistency between extremes for observatories at similar latitudes, there are instances of large differences in return levels, which are unexplained (see Figure 2-2 for an example). For this reason it is useful to put the European results into a global context.

In Figure 2-5 we therefore show the distribution of global observatories, colour coded according to the length of digital data sets each observatory holds (data from INTERMAGNET and the Edinburgh WDC for Geomagnetism). There is clearly an uneven distribution, favouring the northern hemisphere, although the three longest data sets are actually in the southern hemisphere.

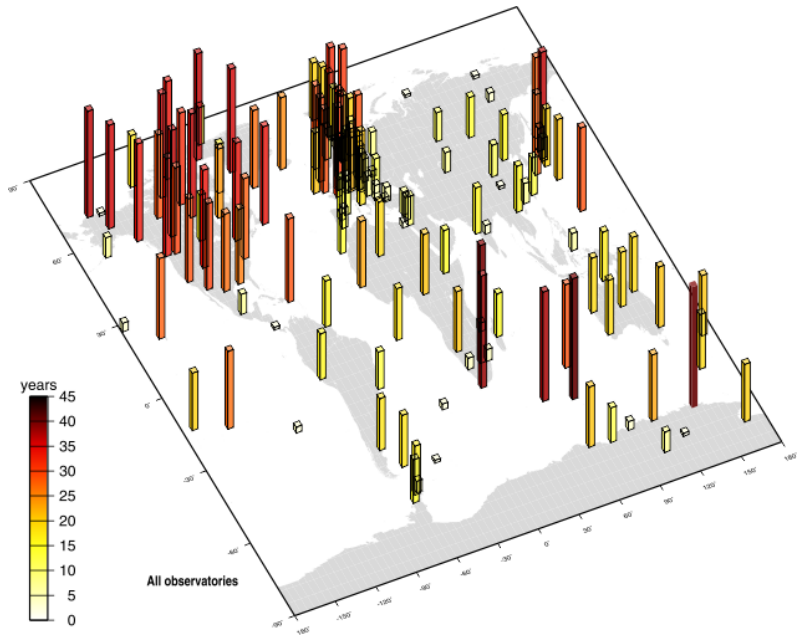

Figure 2-5: Digital data colour coded by duration, for global magnetic observatories.

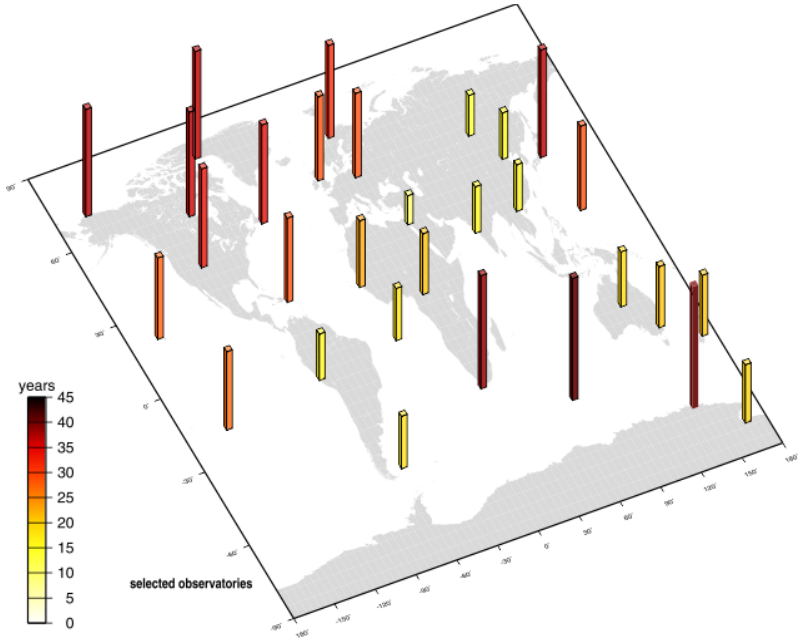

Figure 2-6: Digital data for 30 global observatories, selected for EVS analysis.

Figure 2-6 then shows the locations of 30 observatories provisionally chosen for an EVS analysis. This has a reasonably even distribution in both latitude and longitude, and includes some European observatories for a consistency check with the earlier work. However we note that to obtain this even distribution we find that some observatories have relatively short digital histories. This may impact on the statistical robustness, as was the case in the European study.

EVS has been applied to some of these observatory data sets (this is a work in progress as it requires some laborious quality assurance to remove spikes and outliers). We have analysed the residual minute means – and their rates of change - in the *D*, *H*, *X* (north) and *Y* (east) components, as well as daily block maxima for each component, for context. De-clustering lengths and threshold selections were set as in the previous paper.

In Table 2 we show EVS results for Eskdalemuir from a repeat analysis, carried out by a completely independent researcher, to assess the confidence in the results of Thomson *et al* (2011).

Table 2. Estimated 100 and 200 year maxima in each of *H*, d*H*/dt, *D* and d*D*/dt, *X*, d*X*/dt, *Y*, d*Y*/dt for Eskdalemuir. Data used to compute these extremes are the daily maxima in the one minute observatory data and the maxima per block of 15 minutes. The results from the Thomson *et al.* (2011) paper are shown for comparison with the 15 minute block maxima.

Esk		D	dD /dt	H	dH /dt	X	dX /dt	Y	dY/ dt
100 yr	Daily max	7.11	6.79	3351	1491	3340	1415	2208	1397
	15 Min max	6.62	4.65	4050	4044	3953	3577	3268	1643
	2011 paper	~7.5	~5.1	~5000	~3700				
200 yr	Daily max	9.49	10.93	3938	1892	3949	1781	2908	2014
	15 Min max	8.95	6.94	5195	6668	5051	5798	4916	2500
	2011 paper	~10.0	~8.0	~6000	~6100				

The comparison with the earlier paper is made between the rows labelled ‘minute’ (the new results) and ‘2011 paper’ (published results). Given the wide 95% confidence limits in the earlier work these new results are broadly consistent, which provides confidence in the statistical robustness of our approach. Interestingly comparison with the daily block maximum results (‘daily max’ row) shows some large differences particularly in d*H*/dt and d*X*/dt. This will be investigated further.

Eight observatories have been assessed so far and provisional results are shown in Figure 2-7 for the d*H*/dt component. Even allowing for the relative lack of data (yet) from the southern hemisphere we see a degree of hemispheric symmetry, e.g. as reported by Pulkkinen *et al.* (2012) and Ngwira *et al* (2013a), as well as the 'auroral bulge' of Thomson *et al.* (2011).

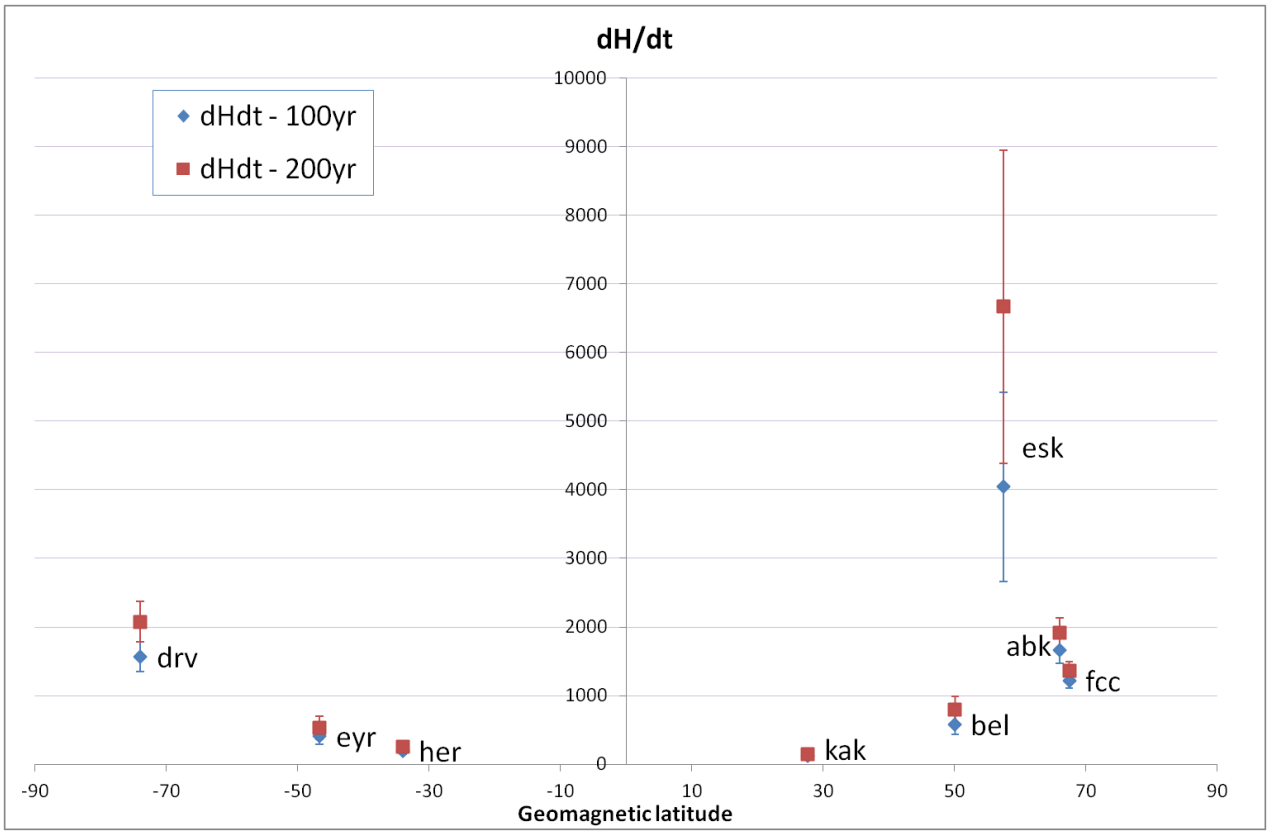

Figure 2-7: d*H*/dt 100 and 200 year return levels using the minute max values, a threshold of 99.97% and a de-clustering run length of 12 hours (plotted by geomagnetic latitude).

One issue that has slowed progress on processing the global data set is the difficulty in selecting a consistent extreme level threshold across all observatories. For some observatories, e.g. Fort Churchill (FCC), we find a high number of occurrences per year (~46) for the rate of change in each component, given a 99.97% threshold. This would suggest that the threshold is maybe not high enough. However for other observatories, e.g. Eskdalemuir (ESK), this is not the case. For this reason we have investigated the trade-off between clustering length, threshold and return level. This is shown in Figure 2-8 for FCC and Belsk (BEL).

From Figure 2-8, for both FCC and BEL (apart from at the 99.97% threshold at BEL) the de-clustering doesn't make much difference to the return levels (i.e. estimates are well within the 95% confidence intervals) and, as the threshold increases, the occurrences per year obviously come down. For FCC the return levels and the size of the confidence interval (range in the plots) increase as the threshold increases. For BEL the opposite is true: both the return levels and the size of the interval decrease with threshold.

What this seems to suggest is that we may need to use a different threshold for *B* and d*B*/dt, in terms of each component and different thresholds between observatories to get a consistent picture. In other words to make sure the GPD fit is appropriate for each observatory separately. This is quite different from the earlier Europe-only study, for which de-clustering length and threshold was fixed for all observatories and all components. For example, we note that in general there are many more occurrences per year for the rate of change of each component compared to the component itself.

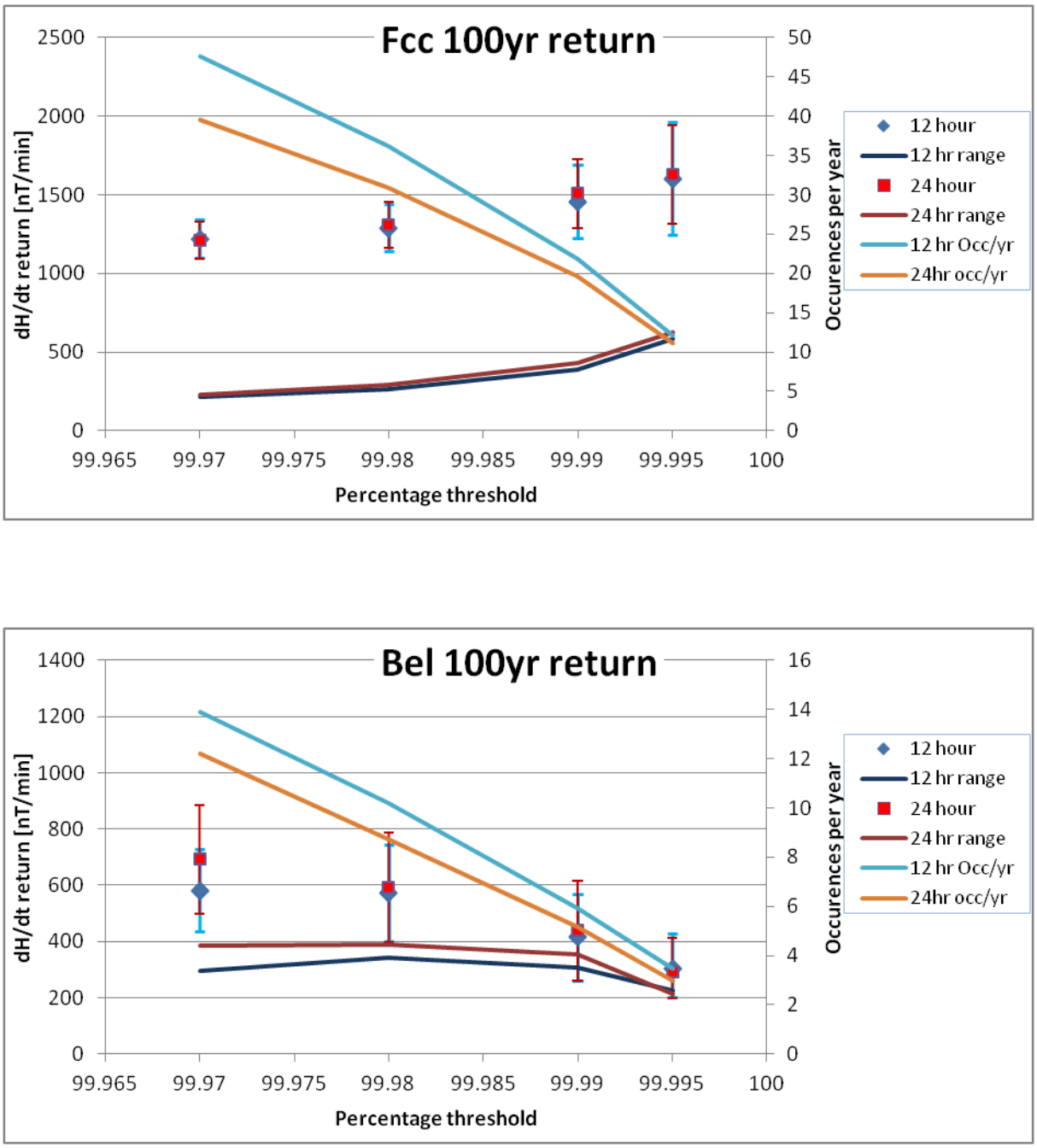

Figure 2-8: The 100 year return levels (left hand scale and blue/red marks and error bars) for a range of thresholds at FCC (top) and BEL (bottom) for the 100 year return period data. The blue and red colourings correspond to 12 hour and 24 hour de-clustering windows, respectively. The dark blue/red lines illustrate the size of the confidence interval. The 'occurrences per year' (right hand axis) indicate the average number of occurrences in each year for values above each threshold (light blue and brown line colour).

2.3 EVS AND NAGYCENK GEOELECTRIC OBSERVATORY DATA

The Nagycenk observatory (Hungary) now has more than 50 years of geoelectric (or telluric) field data. In a poster presentation at the 10th European Space Weather Week, in Belgium, in 2013, Baillie *et al.* (2013) applied the technique of extreme value statistics to these data to determine the 1 in 100 and 1 in 200 year peak values of the surface electric field. These results are very preliminary and are subject to further work, as described below.

At Nagycenk (IAGA code NCK) potential differences are measured using 2m deep, low polarizing, lead electrodes in the North-South (*E*x) and East-West (*E*y) directions, with an electrode spacing of 500 m and data recorded at 1 sec and 10 sec sampling intervals. The data resolution is about 6.1 μV/km.

The following steps were used to process the NCK telluric data:

- Approximately 19 years (Feb 1994 to Aug 2013) of digital data were analysed
- These data were 10-second NCK geoelectric data in *E*x and *E*y, the 3-hour NCK *K* index (geomagnetic activity measure) and the three-hour *T*-index (geoelectric activity measure)
- The data were pre-screened using the local *K* index > 7, producing 106 days to analyse
- For each day a least squares fit, representing the daily baseline, was removed to leave the variations
- The variations were analysed using the eXtremes software toolkit (Gilleland and Katz, 2005) through the *R* statistical package (R Development Core Team, 2008)
- The maximum 10-second values per 3 hour time block were used as the basic data set, providing a manageable reduction in data size, from around 1 million samples to approximately 53,000 data
- A second data set of the maximum 10-second values per day were also analysed for comparison and consistency with the first data set
- The maxima for both *E*x and *E*y were determined for the time-span of data. The projected GPD distribution for periods of 100 and 200 years were computed and the 95% confidence levels in the extremes were also determined

In Figure 2-9 we show comparison plots of *E*x and *E*y for Eskdalemuir and Nagycenk for the storm of 17th March 2013. There are similarities in the data, particularly at longer wavelengths, which is reassuring, but the overall scales are quite different. This suggests, if true also for other storms, that EVS statistics will produce larger return levels for Eskdalemuir, compared to Nagycenk, in line with estimates produced elsewhere by EURISGIC project team members.

In Figure 2-10 we then show two examples of geoelectric data for NCK. Plots of one month of data for a ‘good’ month (top) and a ‘less good’ month (bottom) are shown, with ‘good’ and ‘less good’ defined in terms of the homogeneity and overall data quality. Steps and spikes are clearly visible in the ‘less good’ data and show the need for careful quality control. We note in particular that the *E*-field can be relatively large even when the observatory *K* is only moderately disturbed.

In Figure 2-11 the return level plots for the Nagycenk *E*x and *E*y data, as estimated by EVS are given. Probably the most striking result is the apparent asymptotic upper limit to *E*x, with this being less evident in *E*y. Whether this is physical and a robust result requires further study.

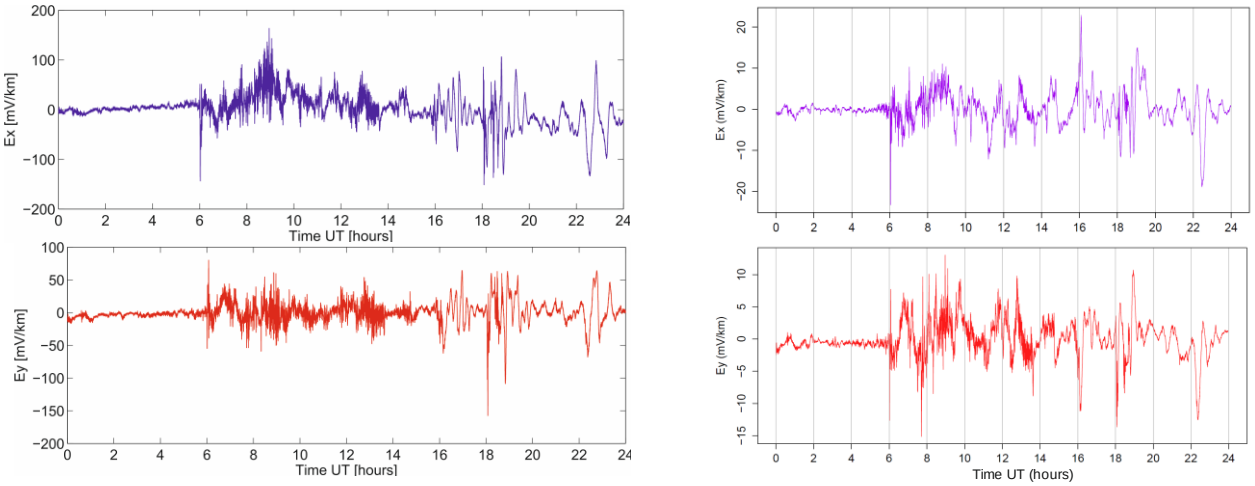

Figure 2-9: Electric field in the north (*E*x) and east (*E*y), for Eskdalemuir (left) and Nagycenk (right), during the storm of 17th March 2013.

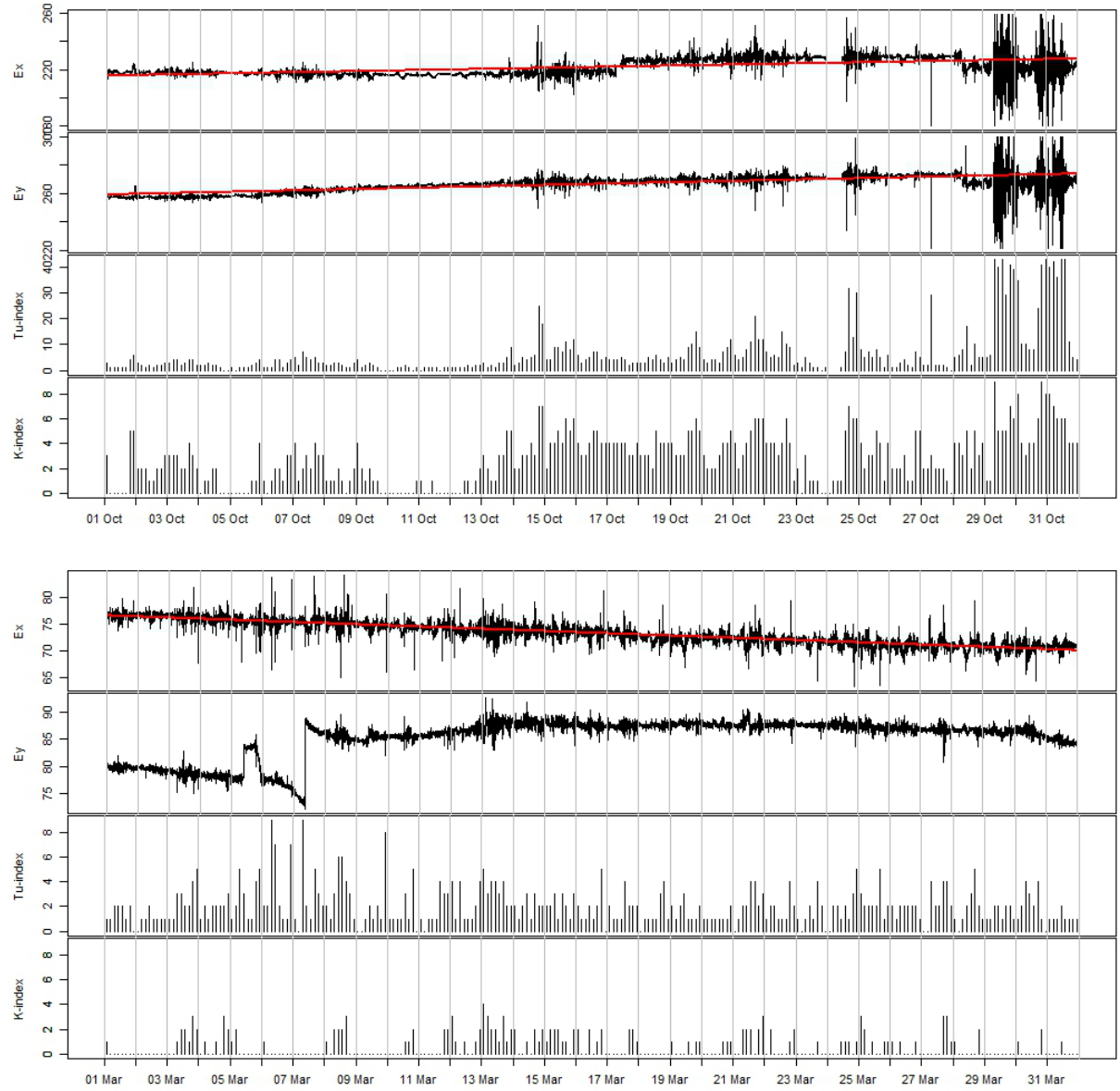

Figure 2-10: Electric field in the north (*E*x) and east (*E*y) directions, NCK *T*-index and observatory *K* index for two months of data, to demonstrate quality control issues when pre-processing the data for EVS analysis.

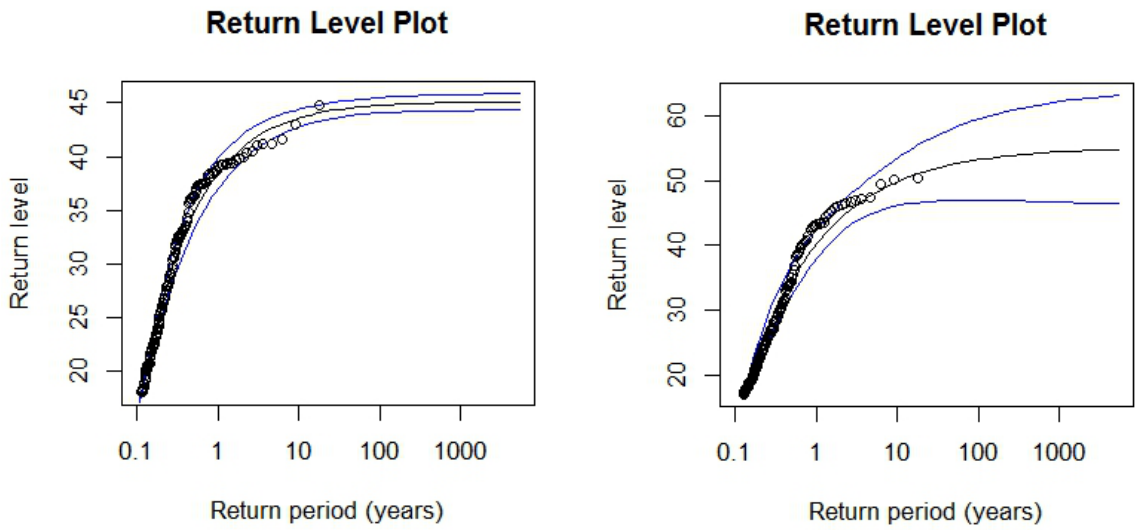

Figure 2-11: Return level plots in the Ex (left) and Ey (right) for Nagycenk. Units for the return level are mV/km. 95% confidence limits are shown in blue. Circles denote measured data.

In summary, what our initial look at Nagycenk data has shown is that

- Both the 100 and 200 year return periods for NCK geoelectric data are about 45 mV/km and 54 mV/km for *E*x and *E*y respectively. These small levels of geoelectric field, compared to Eskdalemuir, may reflect the sedimentary nature of the region and its more conductive nature.
- The return level curves tend to 'saturate' meaning that such 'extremes' are already in the data set. This is unexpected and indicates that further work is required
- Using daily maxima of 10-second data produces similar results (the second data set referred to earlier and not shown here)
- There is a sensitivity of the results to the choice of threshold (currently set at ~33% of the peak level, which is substantially less than for similar treatments of geomagnetic data, e.g. Thomson *et al.*, 2011).

Future work will include:

- Repeating the analysis by including days when the local 3 hour geomagnetic *K* index is 6 (adding ~500 days more for processing and analysis), or through better automated correction of baselines, jumps and spikes
- Repeating the analysis with recently digitised (quality checked) telluric data for more of the 50 years in the NCK record
- Re-computing the NCK *T* index with an unbounded upper limit and analyzing this data set via EVS
- In the long term, comparing results with similar analyses of Eskdalemuir and other UK station data

In 2012, geoelectric monitoring sites were installed at each of the three UK geomagnetic observatories. Data are now being recorded at these sites with the intention, over the long term, of comparing with the Nagycenk data, to provide a wider European scale view of surface geoelectric fields.

For an initial look, in Figure 2-12 we show the distribution of electric field values from the Eskdalemuir observatory, for 1st January to 1st August 2013. It can be seen that there is a long

tail in the distribution, in both the north (*E*x) and east (*E*y) components. Moreover there are clear difference between the *E*x and *E*y channels. This may be physical (local effects?) or may reflect issues with the instrumentation. We note that the local maxima during this time interval (of ~0.2V/km) compare with an estimated 5V/km for central Scotland during the October 2003 storm (Thomson *et al.*, 2005) and even estimates of ~20V/km for genuinely extreme events in resistive geological terranes (e.g. Pulkkinen *et al.*, 2012).

Over time, probably many years, we hope to construct a data set from which we can analyse the tail of the UK distributions using EVS, with a view to confirming, or otherwise, estimated extremes in modeled electric fields, such as given by Pulkkinen *et al.* (2012), or the results obtained from Nagycenk.

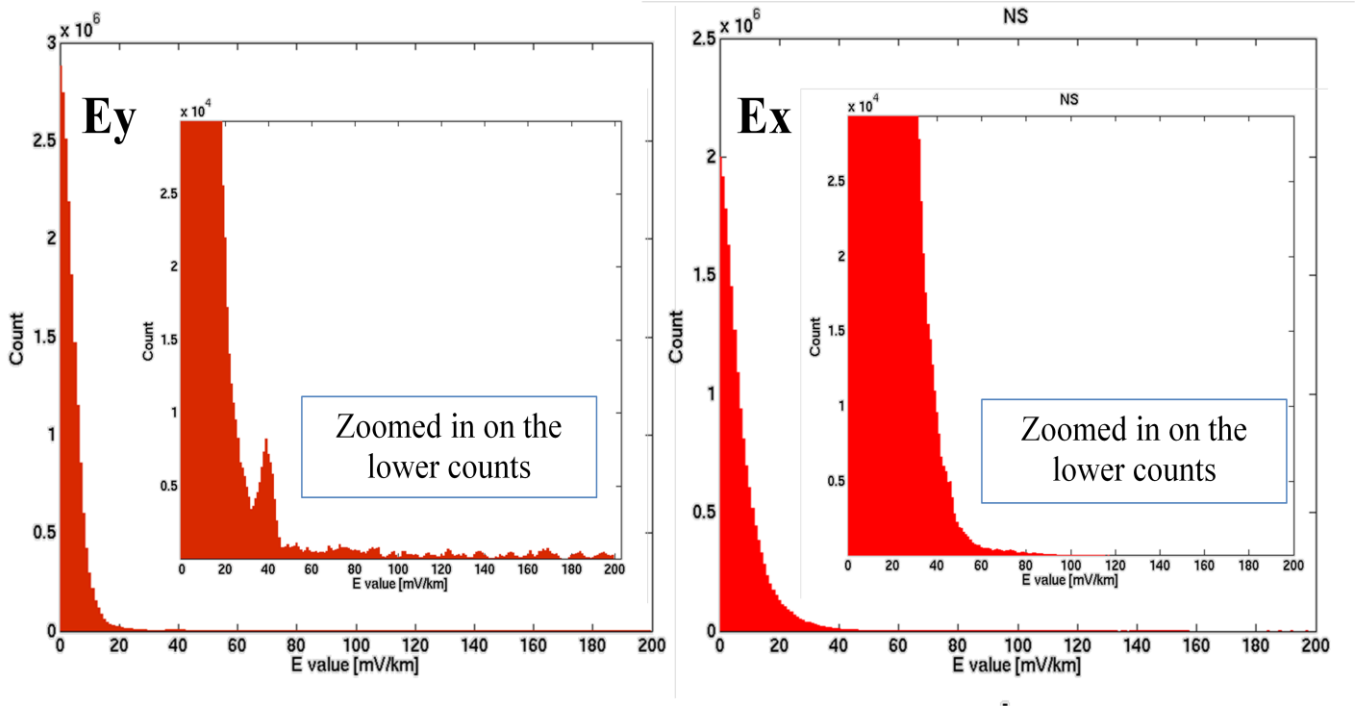

Figure 2-12: Electric field distributions in the north (*E*x) and east (*E*y) directions at Eskdalemuir, for 1st January to 1st August 2013.

2.4 EXTREME GIC IN THE UK GRID

Using the EVS results of Thomson *et al.* (2011), summarised in Section 2.1, Beggan *et al*. (2013) investigated the impact of extreme geomagnetic variations in terms of worst case GIC in the UK transmission system. Beggan *et al.* firstly created an updated model of the UK surface conductivity by combining a spatial database of the UK geological properties (i.e., rock type) with an estimate of the conductivity for specific formations. Secondly, they developed and implemented a sophisticated and up-to-date model for the 400 kV and 275 kV electrical networks across the whole of Great Britain and, in addition, for the 132 kV network in Scotland.

They were then able to deduce the expected GIC at each transformer node in the system based on the network topology and an input 'extreme' surface electric field. Beggan *et al*. applied these developments to study the theoretical response of the present-day UK high-voltage power grid to modeled extreme 100 year and 200 year space weather scenarios and to a scaled version of the October 2003 geomagnetic storm, approximating a 1 in 200 year event. The analysis of Beggan *et al*. derived much from Thomson *et al.* (2005), Beamish *et al.* (2002) and McKay (2003).

As a first hypothetical model, Beggan *et al*. developed two synthetic electrojet model profiles: an electrojet model with an amplitude profile akin to a "top-hat" function, extending from 53N to 63N in geomagnetic latitude, with a second model that had a "tapered cosine" profile extending between 48N and 68N in geomagnetic latitude. They used the two different models to examine if the amplitude gradient (slope) of the magnetic field strongly affects the estimated GIC. The Top-Hat model gave a very strong gradient across its edges while the Tapered-Cosine model had a gentler gradient. Two orientations of the auroral electrojet were computed for each synthetic 100 and 200 year electrojet: (a) geomagnetically east-west aligned across the UK and (b) a geomagnetic north-south alignment (approximately following the central axis of the UK).

To scale each electrojet model to the correct amplitude for an extreme event, the results from the *Thomson et al.* [2011] study on the statistical predictions of extreme values in European magnetic observatory data were applied. Beggan *et al.* used 1000 nT/min, 3000 nT/min, and 5000 nT/min in their analysis to approximate the expected maximum in dH/dt for 30, 100, and 200 years. For an assumed driving sinusoid of period of 2 min, this led to magnetic field input strengths H of approximately 450 nT, 1350 nT, and 2250 nT, corresponding to $d\mathrm{H}/dt$ = 1000 nT/min, 3000 nT/min, and 5000 nT/min.

As a final, more 'realistic' model, a model of the magnetic field during the October 2003 event was constructed based upon the measurements from nine observatories and variometers around the United Kingdom and North Sea region, scaled by a factor of five, again according to the results suggested by Thomson *et al.* (2011). This provided an event with peak magnitude of 5000nT/min at one instant (21:20 UT).

The estimated electric field for the scaled October 2003 model is shown in Figure 2-13. In Figures 2-14 and 2-15 we show the GIC results for Beggan *et al*, for, respectively, the synthetic electrojet models and the scaled October 2003 model.

It is clear that substantial GIC, of more than a few hundred Amps, are possible, according to these scenarios. The largest GIC typically occur in the north of the UK, and in the 'corner' nodes of system (e.g., southwest Wales and England) or in isolated regions (Scottish Borders). Where nodes lie close together, especially in the southern UK, there is a tendency for smaller GIC (e.g., London/southeast England), though this is not necessarily the case with other clusters of transformers (e.g., northeast England). It is also found that any North-South component to the electrojet over the UK (e.g., during a westward travelling surge) will on average increase the GIC flowing in transformer earths. In places, this GIC can be an order of magnitude greater than that for the more commonly East-West oriented electrojet.

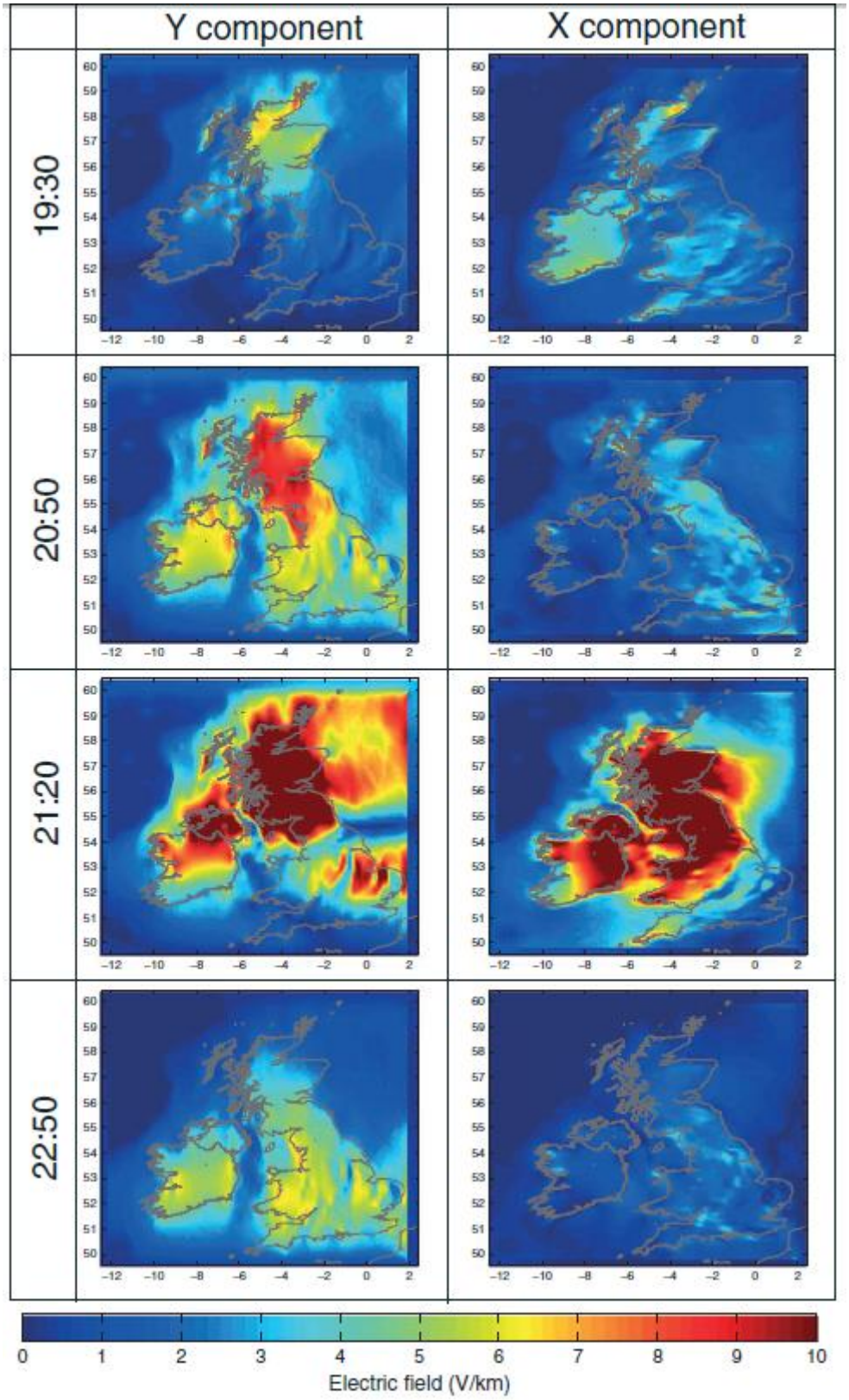

Figure 2-13: Electric field induced in the surface for period of 120 s due to magnetic fields from an extreme version (x5) of the 30 October 2003 geomagnetic storm. The columns show the (left) Y component and the (right) X component. Nominal times (in UT) are illustrative, taken from the time profile of the October 2003 storm.

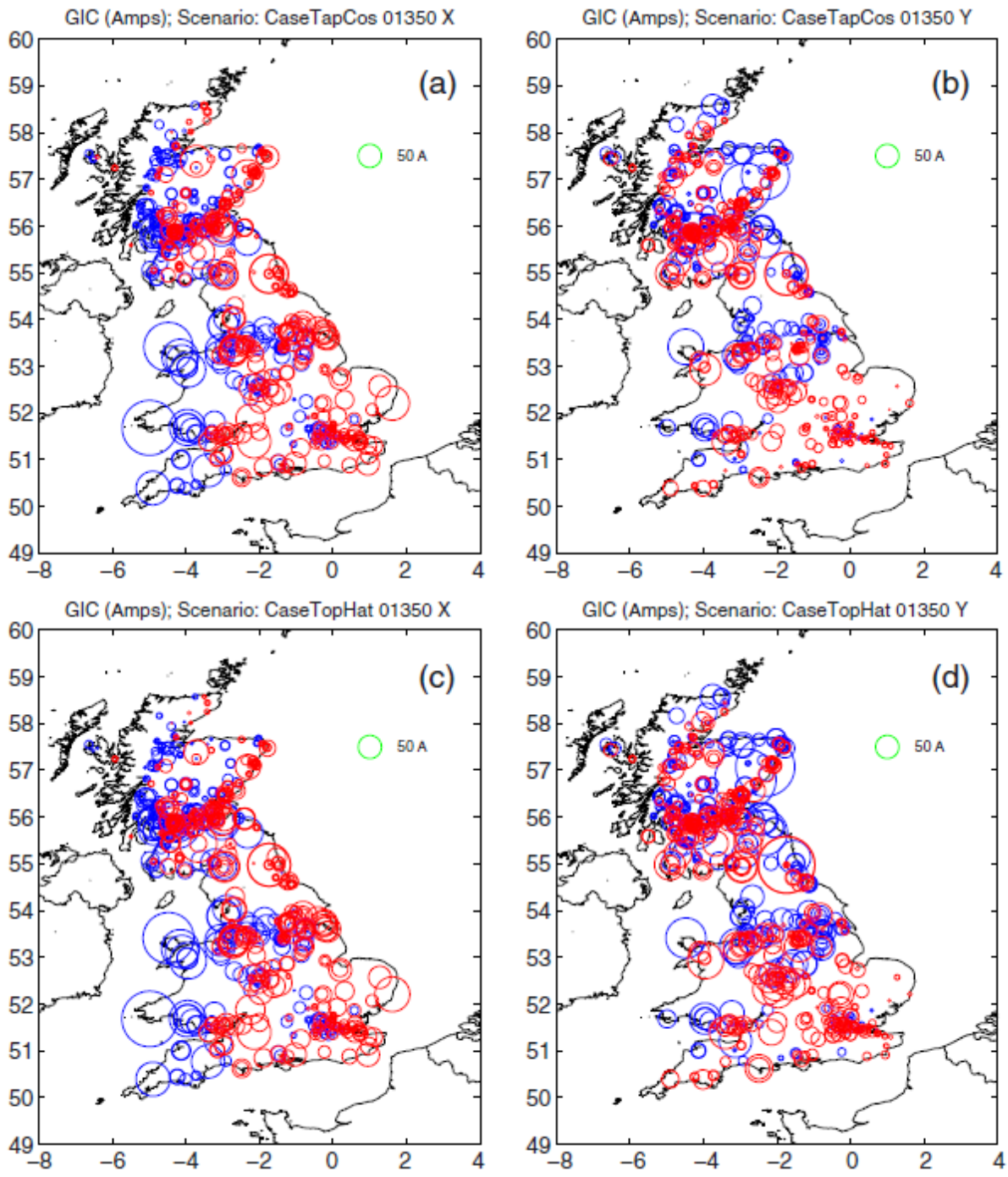

Figure 2-14: GIC in the National Grid GB high-voltage network due to a 100 year extreme scenario (120 s period) from an auroral electrojet with the following configurations: (a) Tapered Cosine East-West aligned, (b) Tapered Cosine North-South aligned, (c) Top Hat East- West aligned, and (d) Top Hat North-South aligned. Blue indicates GIC directed into the grid, red indicates GIC into the ground. Circle size represents size (relative to scale). Note that many sites have multiple transformers present**.**

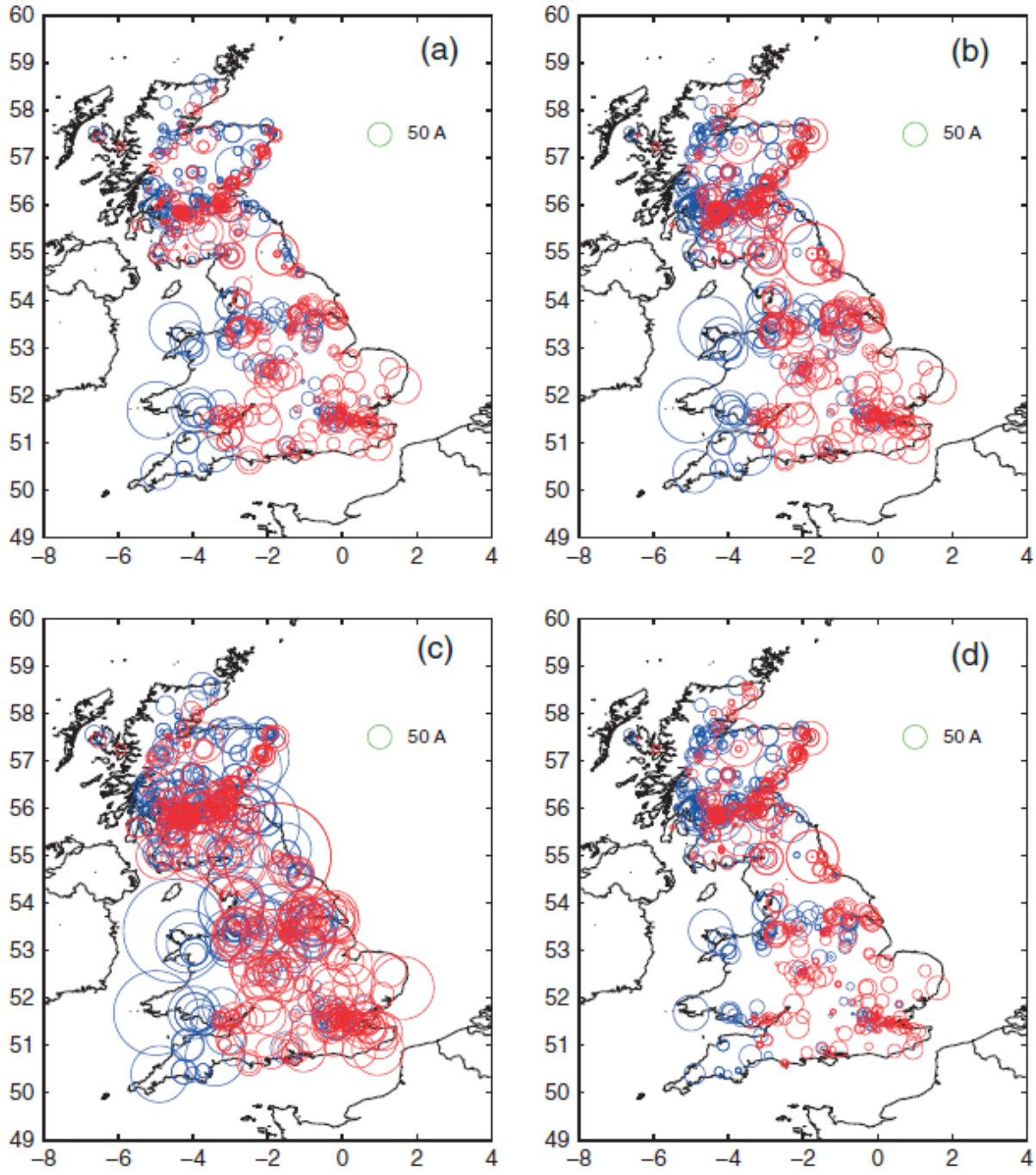

Figure 2-15: Snapshots of GIC in the National Grid GB high-voltage network due to an extreme storm scenario (approximately a factor of 5) of the 30 October 2003 geomagnetic storm (due to an electric field with a period of 120 s). (a) Time: 19.30 h, (b) Time: 20.50 h, (c) Time: 21:20 h, and (d) Time: 22:50 h (see Figure 2-5). Blue indicated GIC directed into the grid, red indicates GIC into the ground. Circle size represents size (relative to scale). Note that many sites host multiple transformers.

3 Worst Case Scenario Research at FMI

3.1 GIC IN THE NORWEGIAN HIGH-VOLTAGE POWER GRID

As an exploitation of existing EURISGIC results, FMI performed an assessment of GIC in the Norwegian high-voltage power grid, together with the Statnett company in 2012-2013 (Myllys *et al*., 2013). The basic results were statistics of the geoelectric field and of GIC based on 10-s geomagnetic data measured in 1994-2011 and on ground conductivity models derived by the EURISGIC project team.

The statistics are based on an 18-year period, which corresponds to about 1.5 sunspot cycles. This is a relatively short time and it does not contain the largest known geomagnetic storms. However to extend the results, we extrapolated the 18-year distributions to determine a once in 100-year case.

We calculated the 10-s electric field values at selected magnetometer stations using the data from 1994-2011. We fitted two curves to the electric field values to estimate the largest magnitude of the 10-s value occurring once in 100 years. Figure 3-1 shows an example for the Tromsø observatory. As a rule of thumb, the once in 100 years field is expected to be about 1.5-2 times larger than that modelled in the period of 1994-2011. The same holds for modelled values calculated from 1-min averages of the magnetic field.

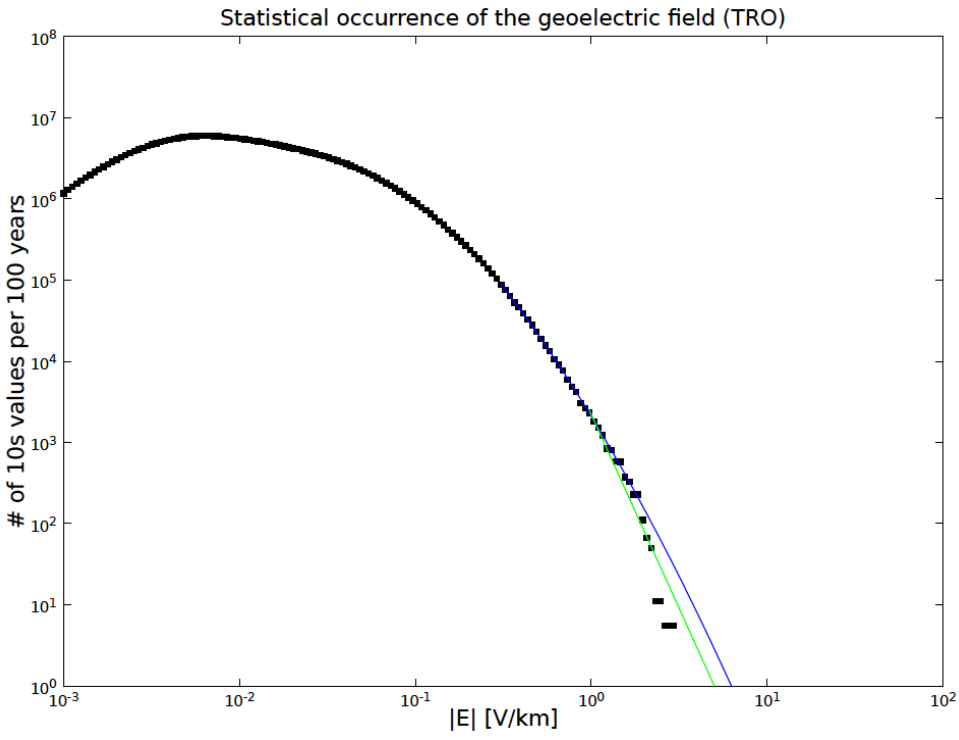

Figure 3-1: Statistical occurrence of 10-s electric field values in 100 years at the Tromsø observatory. Coloured lines correspond to two different extrapolation methods.

Table 3 shows the modelled electric field values at five magnetic observatories during three major storms before 1994. We used 1-min magnetic field values and an identical 2-layer ground conductivity model at all locations. The upper layer of the ground model is 200 km thick and its resistivity is 5000 ohm m. The resistivity of the lower layer is 200 ohm m. With this ground model, the estimated once in 100 years electric field values at Norwegian magnetometer stations

vary between 2 and 10 V/km when determined from 1-min magnetometer data. The largest 1-min field value in 1994-2011 with the same ground model is 4.5 V/km in North Norway.

As Table 3 shows, the electric fields on 13-14 July 1982 reach values equal to the estimated once in 100 year event in Norway at a wide latitude range from Denmark to North Finland. There is also a notably large localized peak value at Brorfelde during the March 1989 storm. Maximum values during the March 1991 storm are also comparable to the Norwegian maxima in 1994-2011.

It seems that the 18-year period of 1994-2011 is too short for assessing extreme magnetic storms. In particular there are at last three magnetic storms in 1982-1991 during which the modelled electric field reaches or exceeds the modelled maximum values in 1994-2011.

Table 3. Maximum time derivative of the horizontal magnetic field vector and maximum of the modelled horizontal electric field at five observatories during three magnetic storms. In all cases, 1-min magnetic field data were used. The same ground conductivity model was assumed at all sites (see text for details).

13-14 July 1982

observatory	max(|$d\boldsymbol{H}/dt$|) [nT/s]	max($\mathbf{E}_{hor}$) [V/km]
Sodankylä (FI)	33.3	7.78
Nurmijärvi (FI)	19.9	8.04
Lovö (SE)	44.8	8.67
Brorfelde (DK)	24.5	6.79
Wingst (DE)	8.0	2.52

13-14 March 1989

Sodankylä (FI)	10.4	3.71
Nurmijärvi (FI)	10.8	3.50
Lovö (SE)	11.7	3.71
Brorfelde (DK)	33.2	9.00
Wingst (DE)	10.7	2.84

24-25 March 1991

Sodankylä (FI)	21.0	4.58
Nurmijärvi (FI)	15.7	5.17
Lovö (SE)	14.1	4.61
Brorfelde (DK)	7.6	1.89
Wingst (DE)	6.2	1.29

3.2 RESULTS FROM RUSSIAN GEOMAGNETIC RECORDINGS IN 1850-1862

We have analysed geomagnetic recordings (Viljanen *et al*, 2013) at four subauroral and midlatitude Russian observatories in 1850-1862 (Fig. 3-2). The data consist of spot readings made once per hour of the north and east components of the magnetic field. We use the hourly change of the horizontal field vector as the measure of activity. We compare these values to data from modern observatories at corresponding magnetic latitudes (Nurmijärvi, Finland; Tartu, Estonia; Dourbes, Belgium) by reducing their data to the same 1-hour sampled format.

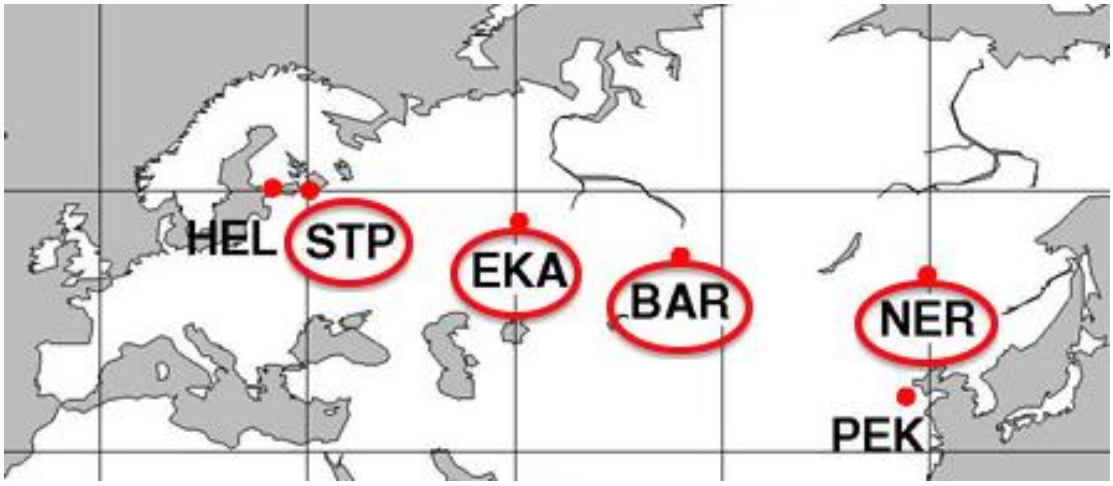

Figure 3-2: Russian geomagnetic observatories in the 1800s. Circled stations were used in this study. Note that there are no digital data from PEK (Peking): there are yearbooks of 1851-1855 but with incomplete coverage.

Geographic and geomagnetic coordinates (CGM in 2000 and 1900) for the circled sites in Figure 3-2 are:

Code full_name lat lon latm2000 lonm2000 latm1900 lonm1900

STP St. Petersburg 59.93 30.30 56.16 106.81 54.73 109.17
EKA Ekaterinburg 56.82 60.58 52.72 133.76 50.39 131.93
BAR Barnaul 53.33 83.95 48.97 156.53 47.22 152.74
NER Nertchinsk 51.32 119.60 45.87 192.42 45.30 188.02

The largest variations at the Russian observatories occurred during the Carrington storm in September 1859 and they reached about 1000 nT/h, which was the instrumental off-scale limit (n.b. identical instruments were used at all the sites). When the time stamp for the spot readings happens to be optimal, the top variation in the Nurmijärvi data is about 3700 nT/h (July 1982), and at Tartu the maximum is about 1600 nT/h (November 2004). At the mid latitude site Nertchinsk in Russia (NER in Fig. 3-2; magnetic latitude ~45 N), the variation during the Carrington storm was at the off-scale limit (Fig. 3-3), and exceeded the value observed at Dourbes (magnetic latitude ~46 N) during the Halloween storm in October 2003. At Nertchinsk, the Carrington event was at least four times larger than any other storm in 1850-1862. The maximum dB/dt at Dourbes during the Halloween storm was about 900 nT/h, so it was smaller than at NER during Carrington.

Despite the limitations of the old recordings and in using only hourly spot readings, the Carrington storm was definitely a very large event at midlatitudes. At higher latitudes, it remains somewhat unclear whether it exceeds the largest modern storms, especially the one in July 1982.

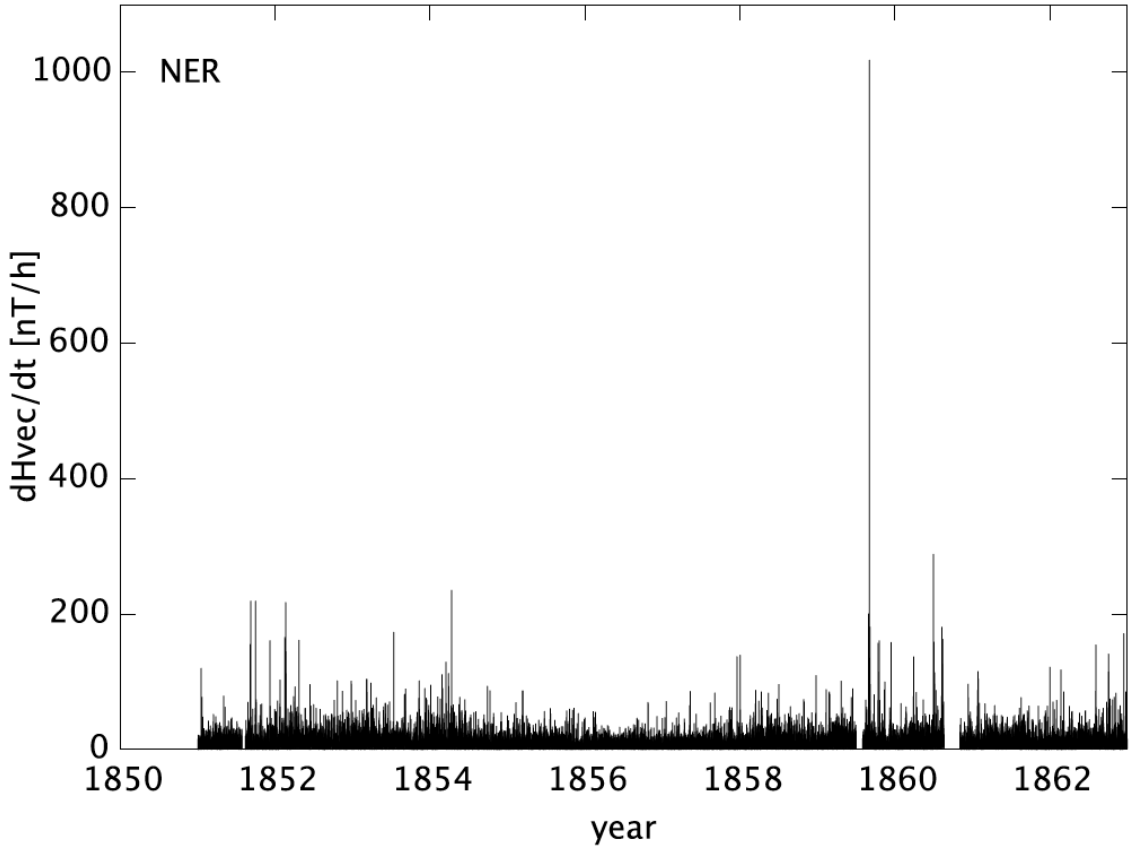

Figure 3-3: One-hour values of the time derivative of the horizontal magnetic field vector at Nertchinsk in 1851-1862. The largest value of at least 1000 nT/h occurred during the Carrington storm in 1859.

4 Worst Case Scenario Research at NASA and Catholic University of America

The worst-case scenarios work at NASA and The Catholic University of America (CUA) has been approaching the problem from three different viewpoints: i) event-based, ii) statistics and iii) theoretical modeling. The event-based and statistics approaches are described in detail in Pulkkinen *et al.* (2012); Ngwira *et al*. (2013a) and for brevity the results are not repeated here. Pulkkinen *et al*. (2012) developed full 1-in-100 year storm and geoelectric field scenarios as a function of local ground conductivity structures and geomagnetic latitudes. Time series representation of the scenarios were provided and applied to power systems in Virginia, US and in UK. The statistics-based scenarios have also been extended to cover all US physiographic regions derived by US Geological Survey (Pulkkinen and Ngwira, 2014).

Later work at NASA and CUA has been focusing on fully first-principles-based investigations of extreme geoelectric field and GIC phenomena. The driving motivation for such studies is that the maturity of modern first-principles-based space physics models allows us to start asking questions about hypothetical extreme storm situations not present in the observational geomagnetic data sets. More specifically, we want to use state-of-the-art space physics models to acquire information about theoretical extremes: how bad can space weather conditions get from the first-principles standpoint? To push our understanding on this topic we have utilized modern space physics model(s) hosted at Community Coordinated Modelling Center (CCMC) for solving the first-principles equations of the solar wind-magnetosphere-ionosphere system under extreme solar wind driving conditions. These solutions allow us to explore also extreme variations of the ground magnetic field and corresponding geoelectric fields. In Sections 5.1-5.3 we describe the NASA and CUA work on the topic.

4.1 USING GLOBAL 3-D MHD SIMULATIONS

The coupling of fast moving CME's to planetary magnetospheres has been a subject of great scientific interest. The magnetosphere is a highly complex nonlinear system whose large-scale state is controlled primarily by the orientation of the interplanetary magnetic field (IMF) and solar wind plasma properties. The transfer of mass, momentum and energy from the solar wind into the magnetosphere-ionosphere system produces various transition layers, the extended geomagnetic tail, and different dynamic current systems and auroral processes.

Three-dimensional (3-D) global magnetohydrodynamics (MHD) models play a critical role in simulating the large-scale dynamics of magnetospheric plasmas. These first principles physics-based models represent a very important component of attempts to understand the response of the magnetosphere-ionosphere system to varying solar wind conditions (see e.g., Gombosi *et al.*, 2000; Palmroth *et al.*, 2004). Upstream solar wind parameters are used as driving conditions for many simulation models of the magnetosphere-ionosphere system, and the results (or performance of these models) are validated by comparing with ground-based or satellite observations. Understanding of the magnetosphere and ionosphere dynamics during extreme solar wind driving is still a major challenge, mainly because of lack of modern scientific data from such periods, as explained by Ridley *et al*., (2006).

4.2 MODELING "CARRINGTON-TYPE" STORM EVENTS

Ngwira *et al.*, (2013b; 2014a) have introduced a 3-D MHD modeling approach with specially refined components for modeling extreme space weather events. The core MHD model is based on University of Michigan Space weather Modeling Framework (SWMF) that uses the BATSRUS code (Powell *et al.*, 1999) to predicts in a self-consistent manner the dynamic

response of the large-scale magnetosphere to changing solar wind conditions. In this study, the low-latitude Colaba estimated minimum negative geomagnetic intensity was used as a benchmark for simulating space weather events that are constructed using extreme upstream solar wind input conditions. Historically, MHD models have typically been utilized for studying non-extreme events. So, the primary purpose of this work is to examine the simulated ground geomagnetic and geoelectric field response during extreme solar wind driving conditions.

We use the SWMF generated ground magnetic perturbations as our primary data for modeling the global ground induced geoelectric field distribution using the plane wave method. On the ground, the simulated CME shows strong geomagnetic and geoelectric field perturbation. Figure 4-1 displays example time series of ground induced geoelectric field components and magnetic perturbations at two active INTERMAGNET ground sites.

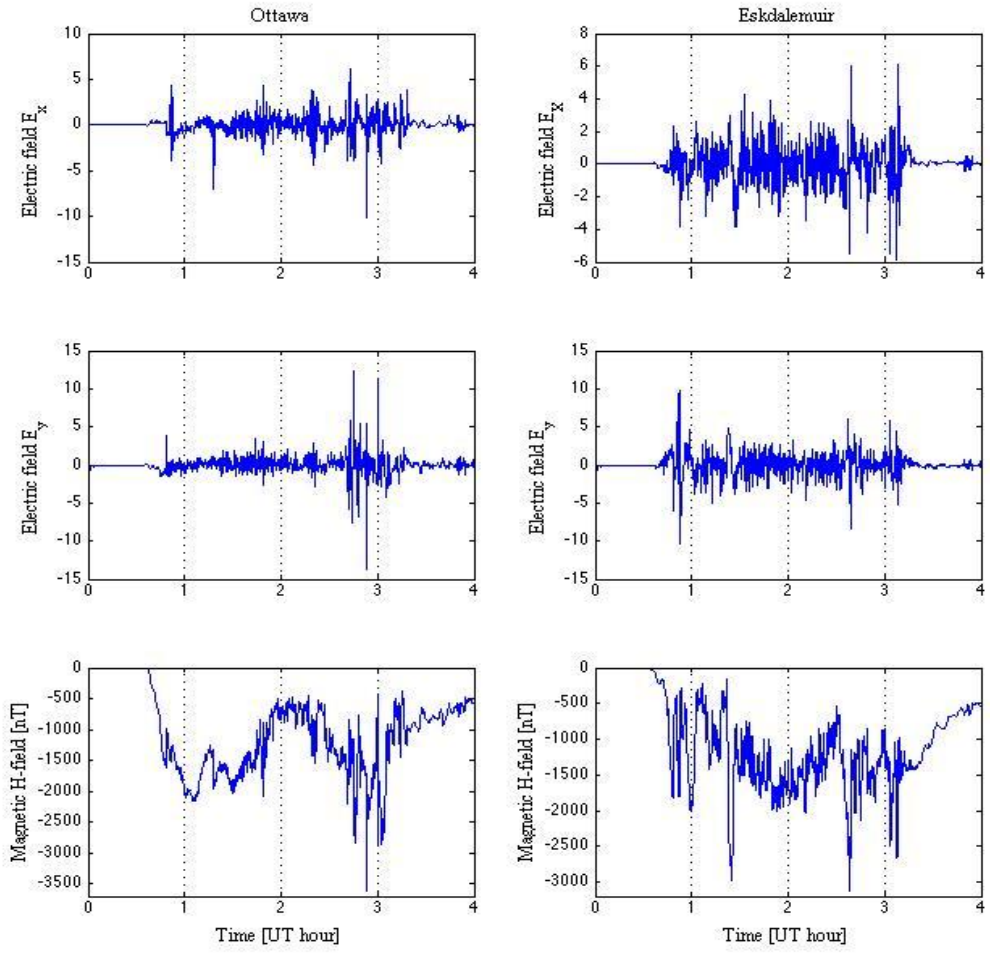

Figure 4-1: Example simulated time series of ground induced geoelectric field components E_x (top) and E_y (middle). Units are V/km. The bottom panels show the simulated time series of the horizontal ground magnetic field perturbations. The two selected high-latitude magnetometer locations are Ottawa (left) and Eskdalemuir (right).

Figure 4-2 shows the distribution of global maximum ground induced geoelectric fields determined for all INTERMAGNET sites. Simulation results for the Carrington-type event are displayed in Figure 5-2(a).. It is clearly evident from the figure that the model is able to reproduce the global geoelectric field distribution.

To further test the MHD model performance, a simulation of a portion of the Halloween superstorm on October 29, 2003 was carried out using the same model settings. Then, we

compared the modeled maximum geoelectric field to the observed for the same portion of the storm event. Results are provided in Figure 4-2(b) showing a comparison for the Halloween storm of the geoelectric field determined from model derived magnetic perturbations (blue) and the geoelectric field determined from observations (red) with a very good agreement. This gives us confidence in the MHD code performance and the results since the model is generally able to capture important features, such as the geoelectric field transition region between the middle and high latitudes.

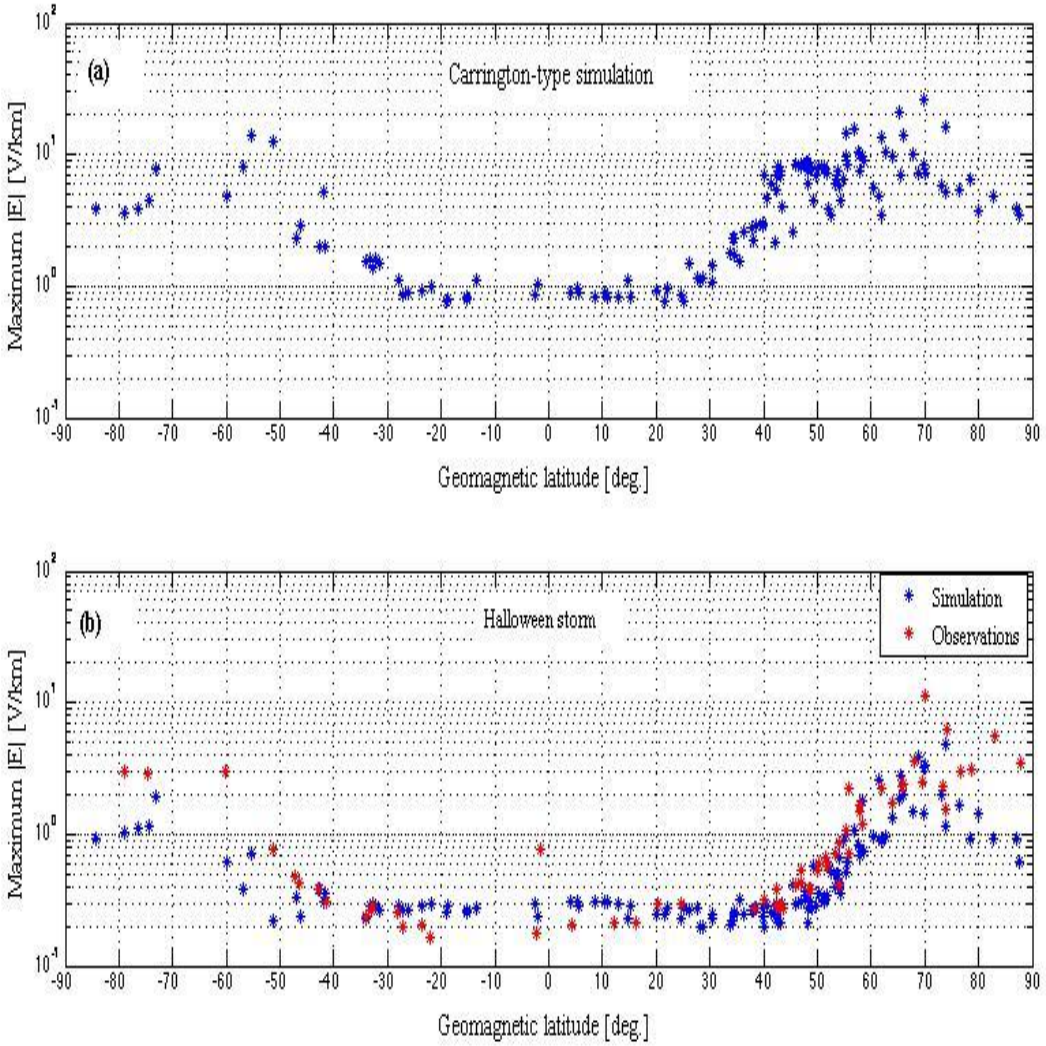

Figure 4-2: Global distribution of the peak geoelectric fields determined for: (a) the Carrington-type event simulation, and (b) for the Halloween storm event, i.e., simulation in blue and observations in red. Each `*' represents a specific ground magnetometer site, and the time of the peak electric field varies from site-to-site. The vertical red dashed lines show the locations of the transition regions between middle and high latitudes.

Additionally, Figure 4-2(a) also clearly shows that the location of the latitude threshold boundary, which is the transition region between the middle and high latitude likely caused by the auroral electrojet current, shifted to 40° geomagnetic latitude. This is much lower than previously determined (50-55° geomagnetic) for observed severe geomagnetic storm events (see reports by Pulkkinen *et al.* 2012; Ngwira *et al.*, 2013a). Furthermore, the strongly shifted latitude threshold boundary implies that the region of large ground induced electric fields is displaced further equatorward due to a shift of the auroral current system, thereby may affect power grids

in regions normally far away from the auroral zone, such as Southern states of continental USA or Central and Southern Europe.

The maximum high-latitude geoelectric field of 26 ± 4 V/km presented in Figure 4-2(a) for the Carrington-type event is in close agreement with predicted theoretical maximum for the 100-year scenario (20 V/km) reported by Pulkkinen *et al.*, (2012).

4.3 MODELING 23 JULY 2012 EXTREME SPACE WEATHER EVENT

On July 23, 2012, a CME was hurled away from the Sun's active region AR1520 with a Rare speed ('R'-type) of approximately 2500 ± 500 km/s (Baker *et al.*, 2013; Ngwira *et al.*, 2013b). This particular CME was not Earth-directed, but was the fastest ever observed in-situ by NASA's STEREO-A spacecraft and had particularly large IMF components (Russell et al., 2013). Events such as the July 23rd, 2012 CME event offer an unprecedented opportunity to explore the effects of extreme space weather. In our study Ngwira *et al.*, (2013b), we considered NASA's STEREO-A spacecraft in-situ observations to represent the upstream L1 solar wind boundary conditions that are used as driving conditions for the global SWMF MHD model. Figure 4-3 shows the interplanetary conditions associated with this CME. Our primary goal was to examine the geomagnetically induced electric field response that this R-type space weather event could have generated had it hit the Earth.

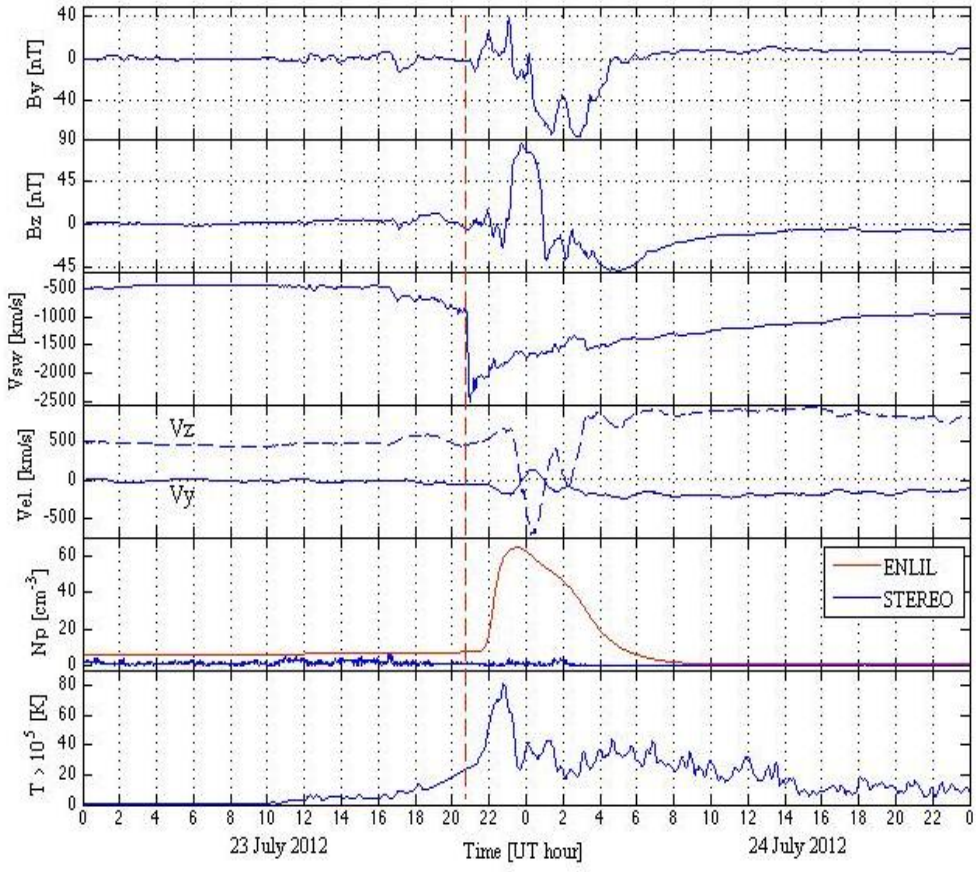

Figure 4-3: Solar wind in-situ observations from the STEREO-A spacecraft. From top to bottom are: the IMF By, IMF Bz, plasma bulk speed (Vsw), the velocity Vy (solid) and Vz (dashed) components, the solar wind density (Np) and the temperature (Temp). Note that the density (red trace) is derived using the WSA-ENLIL 3-D MHD heliosphere model due to challenges in extracting the PLASTIC density data.

Figure 4-4 depicts the maximum induced geoelectric fields at all the individual ground sites used in this study. The figure shows two simulation results, i.e., geoelectric field simulated using STEREO in-situ real-time density (blue) and the other using WSA-ENLIL model density (red). Since our interest is in a worst-case scenario, therefore we only discuss results simulated using the WSA-ENLIL density. Here, the latitude threshold boundary (red dashed line) is located around 50 degrees MLAT and is consistent with observations for severe geomagnetic storms (Thomson *et al.*, 2011; Pulkkinen *et al.*, 2012; Ngwira *et al.*, 2013a). The location of these transition regions between middle and high latitudes is related to the dynamics (strengthening and widening) of the auroral current system Ngwira *et al.*, (2013a).

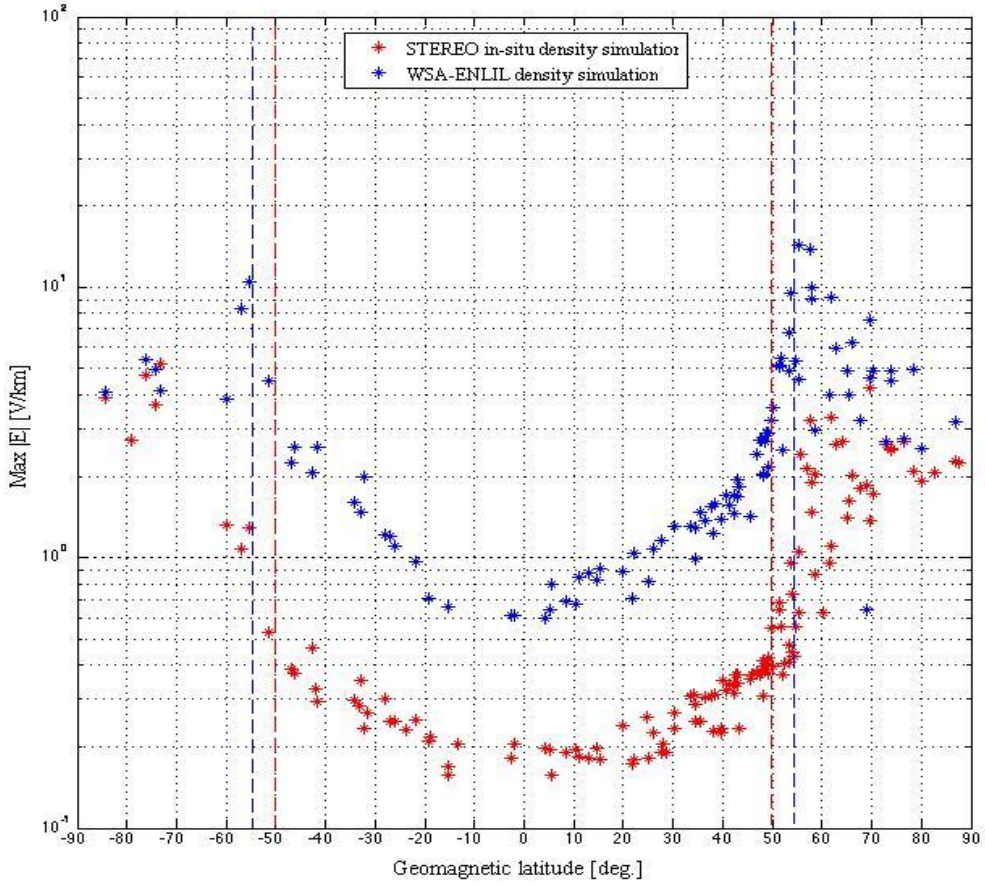

Figure 4-4: The maximum induced ground electric field (blue) simulated using STEREO in-situ density and (red) simulated using WSA-ENLIL model density. Note that the time of the maximum field varies from site-to-site. The red and blue dashed lines show the locations of the mid- to high latitude geoelectric field transition regions, as discussed earlier.

Ngwira *et al.*, (2013b) showed that the largest simulated induced geoelectric fields were observed on the nightside in the European high-latitude sector. One of the interesting features of the result in Figure 4-4 is the value of the maximum ground induced geoelectric field with a peak value of 14.38 V/km. This value is 3 V/km higher than the value determined for previously observed events during the period 1989 to 2005 (11.4 V/km). It was determined by Ngwira et al. (2013b) that the largest geoelectric field peaks were driven by substorm-type dynamics in the simulation.

5 Discussion and Conclusions

It is probably fair to say that at the present time (2013-2014) research into worst case geomagnetic storm scenarios, and extreme geomagnetic events, is still evolving. Partly driven by scientific curiosity and partly by demands from stakeholders, such as governments and industry bodies, there is much activity, but also some degree of convergence, for example, on extreme levels of geoelectric fields and d*B*/dt. However caution is required as there may yet be some new physics or new event data that could still be found. Indeed, digitisation of historical analogue magnetograms (e.g. in WP8 of EURISGIC) is now bearing fruit and may yet change our perception of the meaning of 'extreme'. The geoelectric field results also suggest caution in simple extrapolations, given that some asymptotic maximum level may be present in (some) mid-latitude and sub-auroral data.

However even from the present understanding of extreme geophysical data we can already infer likely extremes in GIC and a number of papers have shown levels in the region of hundreds of Amps per substation, for the UK, Europe and other systems. This is important information for grid operators, in terms of how these Amps are distributed amongst individual transformers of differing type and age. The results also help address whether current levels of 'GIC-proofing' specified for new transformers are likely to be adequate.

It is likely that in the short to medium term that research will continue along the lines indicted in the introduction: through EVS, theoretical and event studies, which in combination will hopefully reveal the true nature of geomagnetic extremes. There are also other data sets for which extreme event analysis is already planned. EVS techniques have not yet been applied to the long record of solar wind data, particularly the southward component of the interplanetary magnetic field. Also, analysis of the complete Nagycenk electric field data is planned, but will take time to process.

References

BAILLIE, O., WESZTERGOM, V., CLARK, E., THOMSON, A., DAWSON, E., NAGY, T., 2013. Extreme value statistics applied to geoelectric activity in Europe, 10th European Space Weather Week, Antwerp, November 2013.

BAKER, D. N., X. Li, A. PULKKINEN, C. M. NGWIRA, M. L. MAYS, A. B. GALVIN, and K. D. C. SIMUNAC (2013), A Major Solar Eruptive Event in July 2012: Defining Extreme Space Weather Scenarios, Space Weather, 11, 1-7, doi:10.1002/swe.20097.

BEAMISH, D., T. D. G. CLARK, E. CLARKE, and A. W. P. THOMSON (2002), Geomagnetically induced currents in the UK: Geomagnetic variations and surface electric fields, J. Atmos. Sol. Terr. Phys., 64, 1779–1792, doi:10.1016/S1364-6826(02)00127-X.

BEGGAN, C. and A. W. P. THOMSON, 2012, Project EURISGIC: UK Regional GIC Studies (Technical Note 1.3). *British Geological Survey Technical Report*, OR/12/024.

BEGGAN, C. D., D. BEAMISH, A. RICHARDS, G. S. KELLY, and A.W. P. THOMSON (2013), Prediction of extreme geomagnetically induced currents in the UK high-voltage network, *SpaceWeather, 11*, doi:10.1002/swe.20065.

GILLELAND, E and KATZ, R. W., 2005. Tutorial for the Extremes Toolkit: Weather and Climate Applications of Extreme Value Statistics, http://www.assessment.ucar.edu/toolkit.

GOMBOSI, T. I., D. L. DE ZEEUW, C. P. T. GROTH, , K. G. POWELL, AND Q. F. STOUT (2000), Multiscale MHD simulation of a coronal mass ejection and its interaction with the magnetosphere-ionosphere system, Journal of Atmospheric and Solar Terrestrial Physics, 62, 1515–1525.

McKAY, A. (2003), Geoelectric fields and Geomagnetically Induced Currents in the United Kingdom, PhD thesis, Univ. of Edinburgh, Edinburgh, U. K.

MYLLYS, M., A. VILJANEN, Ø.A. RUI and T.M. OHNSTAD: Geomagnetically induced currents in Norway: the northernmost high-voltage power grid in the world. Submitted to Journal of Space Weather and Space Climate, 2013.

NGWIRA, C. M., A. PULKKINEN, F. D. WILDER, and G. CROWLEY (2013a), Extended study of extreme geoelectric field event scenarios for geomagnetically induced current applications, Space Weather, 11, 121-131, doi:10.1002/swe.20021.

NGWIRA, C., A. PULKKINEN, L. MAYS, M. KUZNETSOVA, A.B. GALVIN, K. SIMUNAC, D. BAKER, X. LI, Y. ZHENG, A. GLOCER (2013b), Simulation of the 23 July 2012 extreme space weather event: What if the extremely rare CME was Earth-directed?, Space Weather, Volume 11, Issue 12, pages 671–679, December 2013.

NGWIRA, C., A. PULKKINEN, M. KUZNETSOVA AND A. GLOCER (2014), Modeling extreme 'Carrington-type' space weather events using three-dimensional MHD code simulations, submitted to Journal of Geophysical Research.

PALMROTH, M., P. JANHUNEN, T. I. PULKKINEN, , and H. E. J. KOSKINEN (2004), Ionospheric energy input as a function of solar wind parameters: global MHD simulation results, Annales Geophysicae, 22, 549–566.

POWELL, K. G., P. L. ROE, T. J. LINDE, T. I. GOMBOSI, and D. L. De ZEEUW (1999), Asolution-adaptive upwind scheme for ideal magnetohydrodynamics, Journal of Computational Physics, 154 (2), doi:10.1006/jcph.1999.6299.

PULKKINEN, A., E. BERNEBEU, J. EICHNER, C. BEGGAN and A. W. P. THOMSON (2012), Generation of 100-year geomagnetically induced current scenarios, Space Weather, 10, S04003, doi:10.1029/2011SW000750

PULKKINEN, A. and C. NGWIRA (2014), Update on studies of extreme geomagnetically induced current event scenarios, EPRI technical report, in press.

R Development Core Team, 2008. R: A Language and Environment for Statistical Computing, R Foundation for Statistical Computing, Vienna, Austria, ISBN 3-900051-07-0, www.R-project.org. A04204, doi:10.1029/2006JA011900

RIDLEY, A. J., D. L. De ZEEUW, W. B. MANCHESTER, and K. C. HANSEN (2006), The magnetospheric and ionospheric response to a very strong interplanetary shock and coronal mass ejection, Advances in Space Research, 38, 263–272.

RUSSEL, C. T., et al. (2013), The very unusual interplanetary coronal mass ejection of 2012 July 23: A blast wave mediated by solar energetic particles, The Astrophysical Journal, 770:38, 5, doi:10.1088/0004-637X/770/1/38.

THOMSON, A.W.P, DAWSON, E.B., and S.J. REAY, 2011, Quantifying extreme behaviour in geomagnetic activity. Space Weather, 9, S10001. 10.1029/2011SW000696

THOMSON, A. W. P., A. J. McKAY, E. CLARKE, and S. J. REAY (2005), Surface electric fields and Geomagnetically Induced Currents in the Scottish Power grid during the 30 October 2003 geomagnetic storm, Space Weather, 3, S11002, doi:10.1029/2005SW000156.

VILJANEN, A., M. MYLLYS and H. NEVANLINNA, 2013: Russian geomagnetic recordings in 1850-1862 compared to modern observations. Submitted to Journal of Space Weather and Space Climate.